FIRE AND EXPLOSION CONSEQUENCE MODELING IN THE ARCTIC REGION

GHAFFAR KESHAVARZ

FIRE AND EXPLOSION CONSEQUENCE MODELING IN THE ARCTIC REGION

by

©Ghaffar Keshavarz

A thesis submitted to the School of Graduate Studies

in partial fulfillment of the requirements for the degree of

Master of Engineering

Faculty of Engineering and Applied Science

Memorial University of Newfoundland

June 2011

St. John's Newfoundland

Abstract

Pool fires and explosions are among the most frequent accidents in process facilities. For pool fires, flame impingement and thermal radiation are main hazardous characteristic. Whereas, overpressure and negative pulse duration are the main treats to human and assets in the case of explosions. Environmental variables significantly affect the behavior of fires and explosions. However, the effect of environmental parameters in the cold regions like arctic has not been sufficiently studied. This study presents two new models. A steady state and fully developed pool fire model that takes into account the effects of all environmental variables like temperature, the presence of droplets and surface reflexivity on the thermal radiation and subsequently on the fire consequence assessment. Another model has been proposed to account the effect of snow layers on explosion overpressure. A detailed description of model development and solution methodology are presented in the thesis.

Acknowledgments

I would like to thank my thesis supervisors Dr. Faisal Khan and Dr. Kelly Hawboldt, for their patience, guidance and sharing their immense knowledge through this thesis research. I gratefully acknowledge the financial support provided by the Natural Science and Engineering Research Council (NSERC) Canada, and American Bureau of Shipping (ABS) to conduct this research.

I like to thank Dr. Ronald Haynes and Dr. Rouzbeh Abbassi for their helps and precise comments through this work.

I would like to thank my father, mother, brother and sisters for the love, motivation and friendship they have given me every day of my life. Finally I like to thank my friends for their friendships and supports.

List of Tables

List of Figures

Nomenclature

A Area cross section (m^2)
C_p Specific heat (kj/kg.K)
D Diameter (m)
D_d Desired distance (m)
E Energy (kj)
L_c Height of the combustion zone (m)
M Mass (kg)
P Momentum (kg.m/s)
P_o Overpressure (bar)
T Temperature (K)
T_a Ambient temperature (K)
Z Height (m)
Z_0 Height of imaginary source (m)
di Distance (m)
f Mass ratio (product/fuel)
g Gravity of Earth (9.8 m/s^2)
h_c Fuel heating value (kj/kg)
h_v Heat of evaporation (kj/kg)
$\dot{m}$ Fuel burning rate (kg/s)
q Released energy (kj)
q'' Thermal radiation intensity (kw/m^2)
rf Reflection index

Greek Symbols

α Dimensionless correction constant
γ Dimensionless radiation constant
η Dimensionless correction constant
ρ Density (kg/m^3)
ρ_a Ambient air density (kg/m^3)
φ_c Combustion zone equivalent ratio
ω Vertical velocity (m/s)

Superscripts

" . " Average value

Subscripts

c Combustion zone
h Horizontal direction
p Plume zone
r Reflection
v Vertical direction

Contents

Chapter 1: Introduction

1.1 Motivation and Scope

Risk-based design is a widely used and yet growing practice in most of industries. Consequence assessment of the desired fire or explosion scenarios is among the most crucial steps in the risk assessment. There are different methods and models available to preform consequence analysis. These methods and models have been developed and used over years for temperate conditions. Fire or explosion in the arctic region is a unique example of environmentally controlled consequence that has not been studied adequately. The reason is lack of models to include environmental parameters which control the impact propagation. Snow/Ice covered surfaces and the presence of water/ice droplets in the air are such parameters that have not been considered in previous methods and models.

These environmental parameters could significantly affect the consequence of an accident; therefore, the contribution of these parameters must be taken into account especially when consequence is estimated for the arctic region. Hence, studying the effects of environmental parameters and developing new models for fire and explosion consequence assessment are the scope of this thesis. Figure 1.1 illustrates risk assessment diagram and the focus of this study.

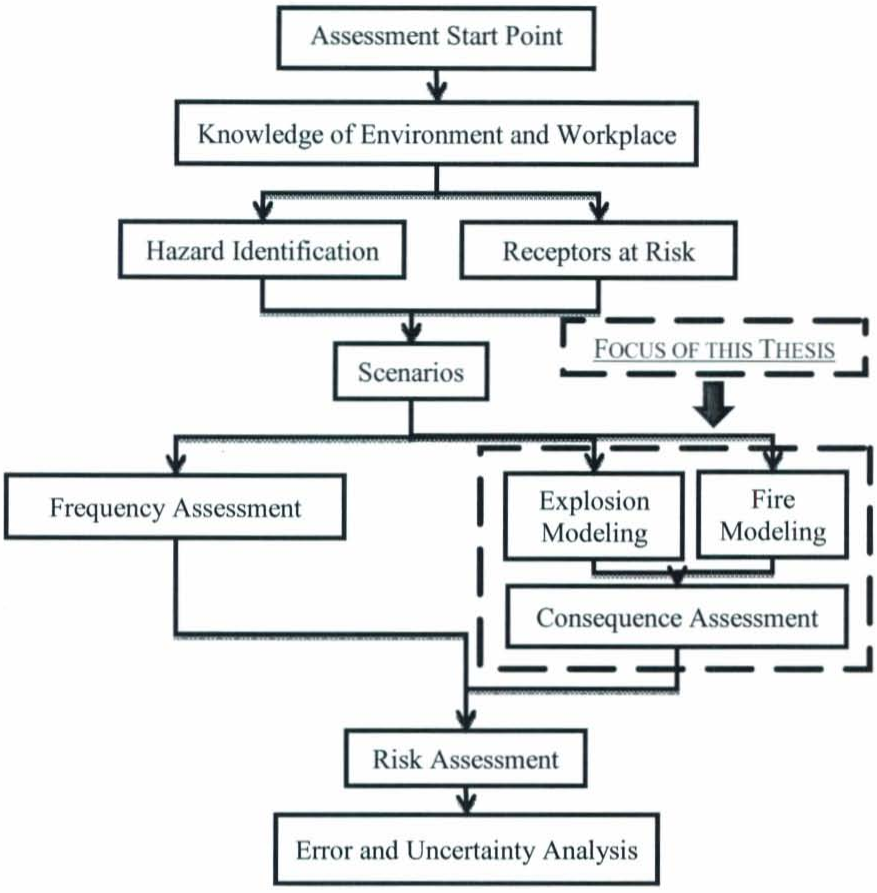

Figure 1.1: The area of focus for this thesis.

1.2 Thesis Outline

Chapter 2 provides a brief description about the arctic region and its main characteristics parameters. Consequence assessment is discussed generally in chapter 3. This chapter explains the procedure of estimating and converting the consequence of an accident. Different categories of fire and different methods for fire consequence assessment have been discussed in details in chapter 4. This chapter discusses different methods, compares them and points out their limitations and applications. Chapter 5 presents the proposed model for pool fire modeling in the

arctic region. This chapter includes the mathematical formulation of the proposed model and literature review of the previous works on the pool fire. Chapter 6 presents available methods and models for explosion consequence assessment. This chapter discusses the advantages and shortcomings of different models. Chapter 7 presents the new model for explosion overpressure calculation in the arctic region. In this chapter, jump equation has been coupled with Baker-Strehlow model. This coupling resulted into order four partial differential equations which have been solved using finite difference techniques. Finally, the contributions of thesis have been summarized in chapter 8. This chapter includes the suggestions for future works.

Chapter 2: Arctic Characteristics

As showed in Figure 1.1, environmental and workplace knowledge is a vital step for consequence assessment. This knowledge contributes to hazard identification and scenario making and subsequently affects the consequence assessment. Variation in the environmental parameters may result into significant consequence differences. For example, thermal radiation of a pool fire significantly attenuates due to presence of water/ice droplets in the air. This chapter briefly indicates the main characteristics of arctic region which make this region different compared to moderate or warm regions.

2.1 Arctic Definition and Boundaries

The Arctic region is the region that surrounds the North Pole which is located within the Arctic Circle (66.5 N) [1]. When defined this way, the most fundamental characteristic of the Arctic region is 24-hour daylight in summer and 24-hour darkness during winter. In spring and autumn, duration of day highly depends on the latitude. During almost all the year, Arctic is extremely cold with much of its land covered with snow, ice, and many areas of permafrost. The environment ranges from large elevated mountains to flat plains, spacious tundra lands and large bodies of water, snow, and ice.

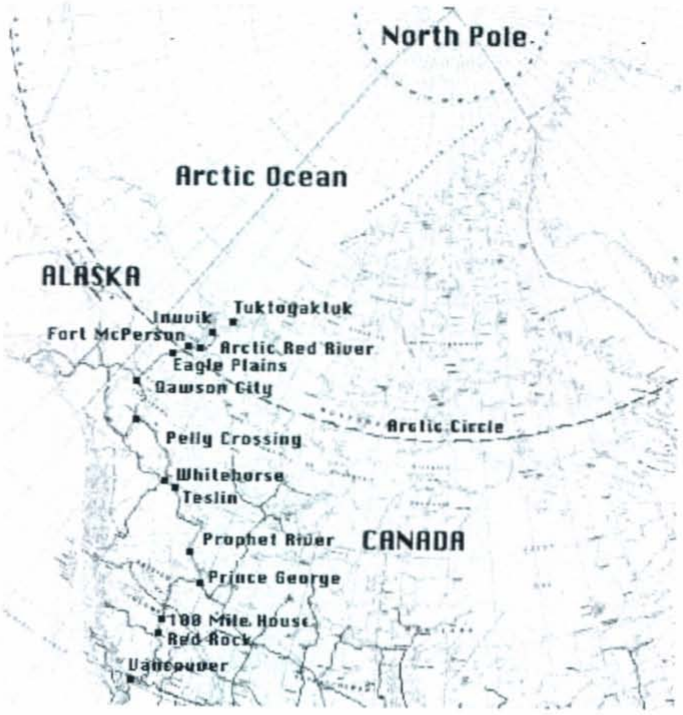

Figure 2.1: Arctic Circle, a major part of Canada and Alaska are in Arctic Circle. Retrieved Dec 13, 2010, from http://www.dom.de/acircle/acircle.htm.

2.2 Snow and Ice

Much of the Arctic environment is covered in enormous masses of ice. The Arctic Ocean is over 1000 meters in depth, and the surface continuously coated with ice [1]. The thickness of the ice usually ranges between 1 to 10 meters with a surface area of approximately 9 to 12 million km^2. About 30 percent of the Arctic Ocean has very shallow water; these parts are known as the continental shelf. Ice sheets are found throughout the ocean surface all year round, but during summer and the end of spring, the ice usually melts at the continental shelf.

In certain areas of Arctic, warm ocean currents increase temperature and moisture content of the atmosphere, causing the amounts of precipitation to increase as well. Some regions can

receive more than 3000 millimeters of precipitation per year such as the Norwegian coast, southern Iceland and Alaska. In other parts of the Arctic where there is no influence of heat, the temperatures are much lower, therefore receiving less than 150 millimeters per year.

Within the central areas of the Arctic Ocean where it is isolated from surrounding influences that may affect the climate, the majority of the precipitation occurs as snow. Although there is rainfall throughout the year, the most rain falls in the warmer months such as in June, July, and August.

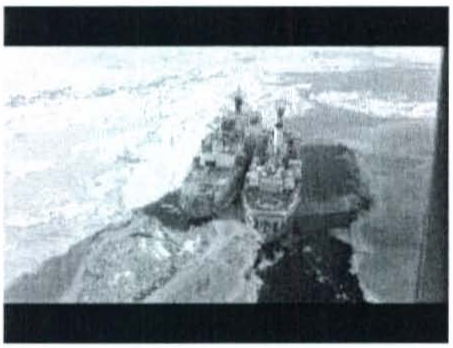

Figure 2.2: Snow and ice covered waters, Arctic region. Retrieved Dec 13, 2010, from http://gallery.usgs.gov/video_tags/seafloor/list/55/1.

2.3 Temperature

The air temperature of the Arctic region is dependent on the solar radiation that it receives from the sun. At locations with higher latitudes, solar radiation is very weak and does not provide too much heat to the environment [2]. Temperatures among locations vary because of the differences in radiation and also from surrounding influences. Usually as the sun rises during the morning, the earth's surface heats up. Sometimes the weather pattern can affect the temperature due to drafts of cold air during the heating process. The cold air flow may cause the

morning temperature to rise slowly, remain the same, or even decreases. The opposite effect can happen as well when drafts of warm air flow results in increase of air temperatures.

When solar radiation interacts with bare land, soil in the ground absorbs it and radiates heat which then warms the surrounding air. In the Arctic region most of the energy is spent for melting large areas that are covered with ice and snow. Especially in the Arctic Ocean, all the solar radiation is used to melt the glaciers; so, the temperature remains freezing cold throughout the day. During the night when there is no influence of solar radiation, the air temperature is manipulated by the amount of cloud cover present. It has been concluded that the temperature is colder during clear conditions and warmer during cloudy conditions.

The annual average of incoming solar radiation in the northern part of the Arctic Circle is approximated to be $100W/m^2$ and the areas located at mid latitude receive a range of 150 to 200 W/m^2. Overall, the Arctic region averaged out to be -34 degrees Celsius in the winter and a range between 3-12 degrees Celsius in the summer seasons.

Surface air temperatures (SATs, approximately 2m above the surface) exhibit remarkable regional and seasonal variability [1, 3]. January average SATs less than −40 ◦C characterizes parts of Siberia. Over the central Arctic Ocean, winter temperatures are somewhat moderated by heat fluxes through the ice cover. January mean values of −25 ◦C to −32 ◦C are typical [1-3]. During July, mean values over snow-free land surfaces are typically 10 ◦C to 20 ◦C [1-3]. Over the central Arctic Ocean, the presence of a melting ice surface keeps summer temperatures close to zero.

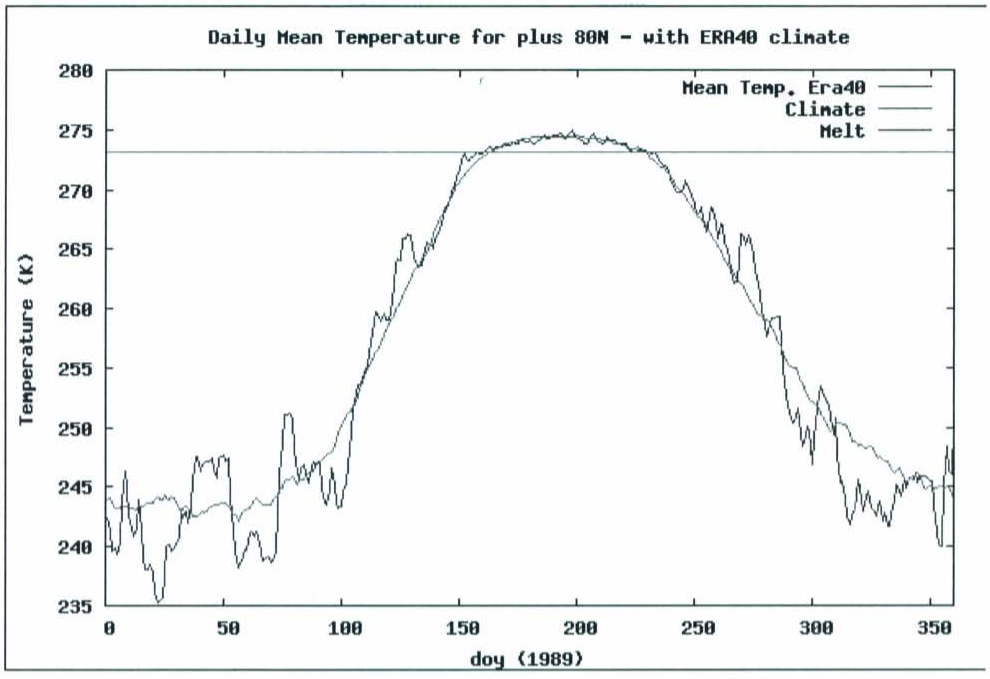

Figure 2.3: Temperature variation during a year in plus 80 N, Retrieved Dec 13, 2010 from https://climatesanity.wordpress.com/category/arctic/ .

2.4 Wind

During winter the Arctic region is known to have high winds with snowstorms between calmed periods [1, 4]. With high velocities, the Arctic winds gather snow as it flows through large open spaces and deposits it in sheltered areas. Winter wind speeds are usually slower than summer wind speeds due to frequently occurring inversions, and surface winds are separated by the inversion layer from the strong upper layer winds. Wind speeds that blow from the west are also normally slower than the winds that blow from the east.

Arctic winds usually blow in from the west as part of the westerlies. Depending on the topography, there are influences among wind strength, direction, and temperature. As wind

flows through coastal channels or mountain passes, its strength can be increased. Katabatic winds flow downward which can be warm or cool according to the situation, forming over glaciers in mountainous areas from high to low grounds, accelerating on the way down. Anabatic winds are usually warm as it flows upward due to the rising of air, frequently forming as air flows off a body of water. Anabatic winds are usually very light, more known as a summer breeze.

Near-surface winds are typically light in the central Arctic with mean annual speeds averaging 4–6 m/s [1, 4]. The NP observations show mean speeds of about 5m/s year round. At stations in the Canadian Arctic, mean wind speeds are typically less than in the Russian Arctic due to the lower frequency of cyclone activity. Nevertheless, when they occur, they may last several days with extremely high speeds exceeding 25 m/s [1, 4].

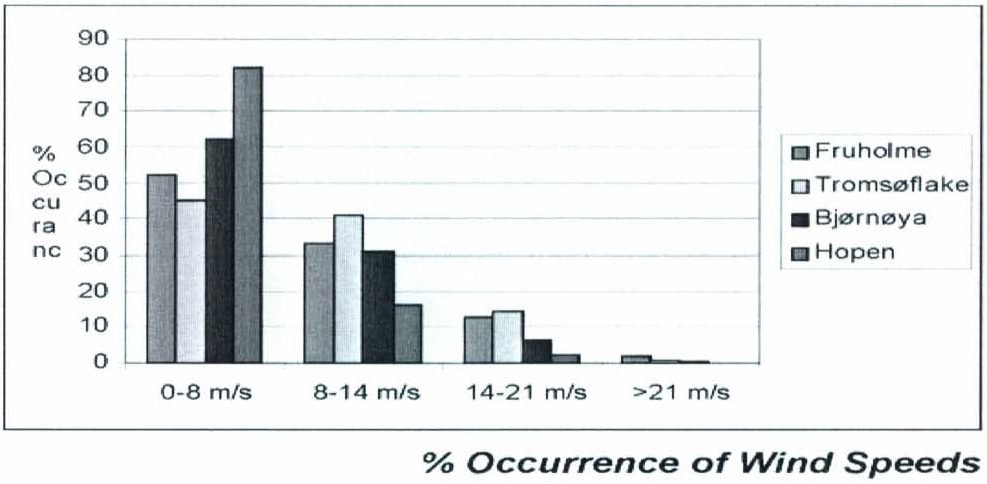

Figure 2.4: Frequency of wind velocities in Barents Sea. Retrieved Dec 13, 2010 from http://www.barentssea.no/?p=barentssea&l=en .

2.5 Fog and Visibility

Fog causes a major visibility problem in the Arctic. There are different types and some of them are known as advection, radiation, and ice fog. Fog is most often found along the coast parallel to the shore. During the winter season, the land is much warmer than the surrounding water. As warm air from the water flows over the cool land, the air of opposite temperatures mix to form fog. In the summer season, the same thing occurs except the air from warmer lands and cooler waters mix instead. Ice fog creates fog the same way except that it consists of ice crystals rather than water droplets, usually occurring at temperatures below -45 degrees Celsius.

Cold air inability to hold moisture causes sea smoke during winter seasons. The temperature of air is significantly lower than water and causes steam to rise. A blanket of water droplets is formed by the steam which is considered to be sea smoke. Sea smoke is known to be another type of fog, formed in a similar fashion and having the same visibility effects.

Another visibility problem in the Arctic region is called Arctic haze. Characteristics of Arctic haze consist of limited visibility in the horizontal directions but clear visibility in the vertical directions. It is known to be formed from very small ice particles since it reflects many different colors as light interacts with the haze. As sunlight shines through the haze, it is known as diamond dust because of all the rock-like particles, but near the ground it appears to be mist or smoke [1-3].

2.6 Humidity

Arctic air is expressed to have very low temperatures and moisture content. During the winter, air is significantly colder and dryer over land than it is over water. Since water is warmer than land in the winter, the air above picks up water particles as it flows across the surface and

retains its higher temperature values and moisture content [5]. On average the Arctic relative humidity found at the surface is ranged from 50 to 60 percent. Near the surface, mean specific humidity (mass of water vapor per unit mass of air, including the water vapor) for winter as averaged for the region north of 70◦ N is only about 1 g kg^{-1} compared to about 3 to 4 g kg^{-1} in summer [1].

Chapter 3: Consequence Assessment

Previous chapter briefly pointed out the main characteristics of the arctic region. According to these characteristics and workplace characteristics/geometries, scenarios are defined. Once scenario are defined, they are analyzed for consequence and likelihood assessment. Consequence assessment refers to attempts toward quantification of hazard intensity. Among hazardous events; fire and explosion are the most common accidents in oil and gas industries. Fire is more frequent; in contrast explosion has higher damage potential and commonly leads to fatality, injury and property loss. The consequences are usually calculated in terms of production loss, human health loss, assets loss, and environmental damages.

Consequence assessment helps to determine the potential damage due to hazardous occasions; however, but does not account for how frequent the accident occurs. If the results of consequence assessment are not directly quantifiable, then it has to be converted to some measurable impacts (monetary terms usually).

Integration of all identified losses (e.g. production loss, asset loss, human health and safety loss, environment loss, information and knowledge loss) to obtain the overall consequence of a hazardous event requires special treatment [6-8]. Figure 3.1 shows the flowchart for an overall consequence with different categories.

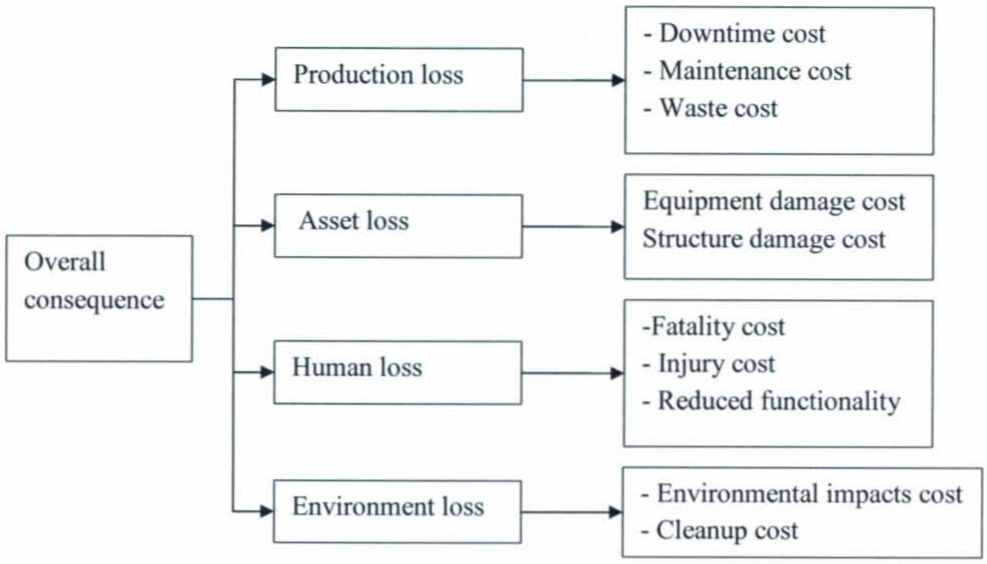

Figure 3.1: Overall consequent with different categories.

3.1 Methods for Consequence Assessment

Scenarios are identified according to the consequences of hazards, in terms of the probable fatalities, injuries, damages, and failures that can be determined in three different ways [6-9]. Available methods can vary from highly subjective methods like engineering judgment to highly computational methods using computational fluid dynamic (CFD) tools.

Historical data can be used to evaluate consequences. The scenario can be compared to accidents of the past that had similar hazards. For example, reviewing the last accidents will help to show the trend of consequence and its intensity. Moreover, it helps for a better understanding of the consequences for specific events, and breaks down the damage outcome of each consequential effect. Historical data may be specific to the environment of the incident, specific to structures of a similar type sharing the same general location or owner.

There are advantages and disadvantages for estimating consequences with historical data. The data helps support the values given in a specific accident to calculate the consequences, if they are sufficient enough to give precise results, data from these past incidents can be used to make a reasonable risk assessment. Though this may be practical for average valued results that have a set number of variables, experiments that have a large number of variables are not accounted for, and outputs a significant difference in data. The incidents used in comparison should have very similar structures for the best results. Another problem that may arise is the errors or change in data over time which discourages the use of the information previously collected.

The size of databases is a major contribution in consequence estimation, more data is available as it increases in size. Though there may be sufficient data, the information needed to be accurate. Often, the details provided are not all the details required for consequence estimation. Historical data is rarely complete because minor incidents that could have led to major incidents are not always recorded. to use historical data, the relevancy of the data must be determined and if it is suitable to be studied. (If applicable, then apply, if partially, apply judgment to modify data, and if not, use another method)

Engineering judgment is another useful way to evaluate consequences. This method is limited to judgments or opinions that are of engineering expertise, in order to have consistency in results. Engineering judgments may be based from the previous experience of another practitioner or from the use of an organized and reliable process such as the Delphi method. This process is very practical because it provides estimation that is completely inexistent or lack in other methods. The Delphi method causes problems for most practitioners as it requires skill and experience to be used.

Another disadvantage from the use of engineering judgment is bias opinions; they arise from various individuals according to what has happened in the past. Thus always the opinion of several experts must be asked and an individual opinion cannot be relied on lonely. Subsequently this results in a range of estimations and potential outcomes. Although this method does not provide a point value, sometimes the inaccuracy is fine when a range of values is of interest instead of a specific estimation.

Models have been developed to evaluate accident consequences; they can calculate the number of deaths or injuries, loss, cost of downtime or business interruptions, and also any environmental damages. Fire models are normally capable of evaluating fire development, smoke movement, structural response, and evacuation response, while estimating the time it takes to reach its critical damage threshold. Likewise explosion models are able to estimate dispersion, flame propagation and generated overpressure. These models are used for quantitative estimates based on rationalized methods and any changes in the design are related to the consequence results; therefore, allowing designers to acknowledge where changes should be made to minimize risk.

Accurate input values are sometimes hard to acquire due to uncertainties. Depending on how complex the problem may be, one simple model cannot provide all the required results and need to be combined with other models. When using one model at a time, the results of one may be used as input data for another as a sequence, and if mistakes are made in the beginning, the entire process will be incorrect. Figure 3.2 shows available methods for consequence assessment and their advantages and disadvantages.

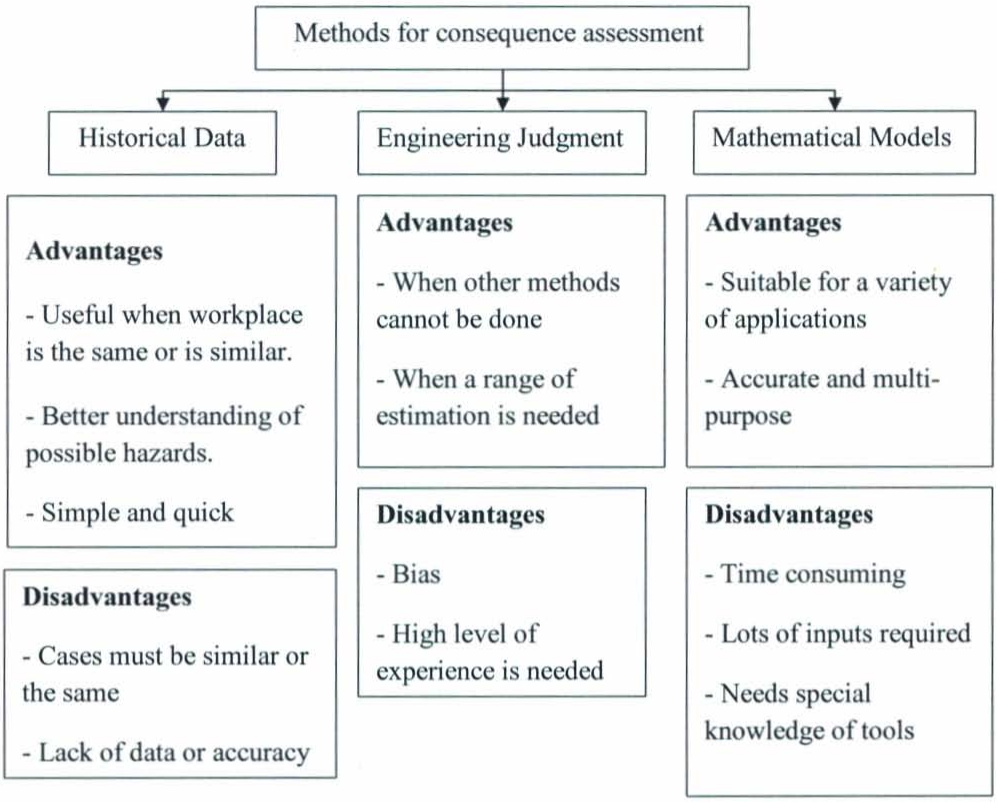

Figure 3.2: Available methods for consequence assessment

3.2 Converting Consequence to Measurable Impacts

Consequences caused from accidental fires and explosions are measured in different ways. This includes the measure of health and safety impacts, loss of property, business disturbance costs, or environmental damages. The consequences can be subjective or objective, and can be caused by direct or indirect factors and must be identified during the risk assessment to do a reliable risk assessment.

Evaluating consequence is more difficult compared to evaluating hazards, in a way that the value of loss or harm may be unclear and hard to determine. While life safety consequences are

estimated, injuries and loss of human life are included in the criteria but a lot of the time other important factors are not included. Factors such as lower quality of life, pain and suffering, rehabilitation after a fire related incident, inability to work after an accident, and effects on family support. There are other long term concerns that include loss of image and market shares for a specific business. Such impacts are very complicated and in most cases are not considered as a part of consequence assessment.

Chapter 4: Fire Modeling

As discussed in previous chapter, there are several methods to estimate consequence of an accident. Among those methods, mathematical modeling is recognized to be the most powerful method due to its flexibility and ability to handle different level of complexity and details. Available methods may be divided into two main categories based on their outputs: physical models and effect models. Physical models calculate variables which are direct outcomes of a hazardous event. For example they may estimate parameters like temperature, radiation, toxic gas concentration. Effect models convert the outcomes of physical models to more sensible impacts like fatalities, injury or loss of property.

Models may be classified as empirical and computational. Empirical tools estimate parameters based on experimentally obtained correlations; thus, a short time is needed for calculations. The assumptions and limiting conditions during the derivation of these correlations, limit the application to simple geometries. In contrast to empirical tools, computational tools take advantage of governing equations in estimating desired parameters. Although it takes a much longer computational time to run these models, the result is expected to be more accurate and reasonable. These models have the ability be applied for complex geometries where the application of simple empirical models might be meaningless.

Although there are numerous models available for consequence modeling, selecting the most suitable model is not an easy task. In selecting a model all workplace, environment condition and different scenario must be considered and the selected model must have the ability to take into account these conditions. For example the FRED may be used to estimate impacts of a hazardous event in a simple geometry; however, it is not applicable if reflective surfaces such as snow

present. **F**ire, **R**elease, **E**xplosion and **D**ispersion (FRED) is a software developed by Shell for quick estimations based on the experimental data.

4.1 Fire Categories

The main cause of injury or damage from a large open hydrocarbon fire is thermal radiation. The different types of fires behave differently and exhibit markedly different radiation characteristics. Radiation and convection are the principal mechanisms for transferring heat from a fire to a structure. The radiation is usually the dominant mode of heat transfer, although convective heat transfer becomes an important mode for structures directly impinged or engulfed. Typically, fires can be classified into four categories: pool fires, jet fires, fireballs and flash fires. In a pool fire, the pool of vaporizing fuel forms buoyancy controlled turbulent flame where the fuel vapor has negligible initial momentum. Pool fires occur from the accidental release of liquid fuel during loading of tanks or due to rupture and/or fracture in pipes and tanks. The probability of occurrence for this type of fire depends on the type of fuels and environmental conditions. Heavy fuels are most likely to produce pool fire while light fuel may evaporate and produces vapor cloud. In warm environments fuel will mostly evaporate while the same fuel may generate a pool fire in cold environments like the Arctic.

Jet fires occur due to immediate or quick ignition of pressurized fuel. This fuel could be a single phase of gas, gas and liquid and even sometimes liquid [10-12]. Jet fires are much more dangerous than pool fire because of the radii of its impacts. Depending on the scenario specification (released phase and angle of release) jet fires can be horizontal or vertical. Horizontal jet fires are more hazardous especially downwind. Jet fires may lead to impingement of structures, equipment and vessels, rupture of pipes and secondary failures.

Since jet fires have high radii of impact, scenarios which include jet fires should be specified precisely because of domino effects. The domino effect is the situation when an accidental fire triggers and expands fires to the other parts workplace. This is an extremity hazardous event when the installation is highly congested due to limitation of space like offshore structures and ships. In those places, jet fires lead to a very high rate of heat transfer and rapid deformation/destruction of structure.

The domino effects of pool fires or jet fires may increase the pressure inside a tank which contains flammable compounds. The increases in temperature and pressure may result in tank failure due to boiling liquid expansion vapor explosion (BLEVE) [13, 14]. In this situation, due to a sudden pressure drop, liquid evaporates and ignites. This results in an overpressure and missile hazards. Furthermore, this results in a higher thermal radiation compared to jet and pool fires.

Due to the thermal radiation, overpressure and missile hazards, BLEVE could be more hazardous than other types of fires. If the tank contains gas, this may result in a very large and rapid fireball. Such a fireball has the highest thermal radiation profile among all different types of fires. The fireball shape, behavior and size are strictly related to type of fuel, failure mode and failure time.

A flash fire is a type of fire in which there is a short delay between the release and ignition times. In this category of fire, the gas or vapor cloud is released and then is ignited; thus, there will be a negligible overpressure. Flash fires are transient and result in a temporary heat radiation. However it could trigger other types of fire especially if flame turns back to the source. Figure 4.1 summarizes the categories of fires.

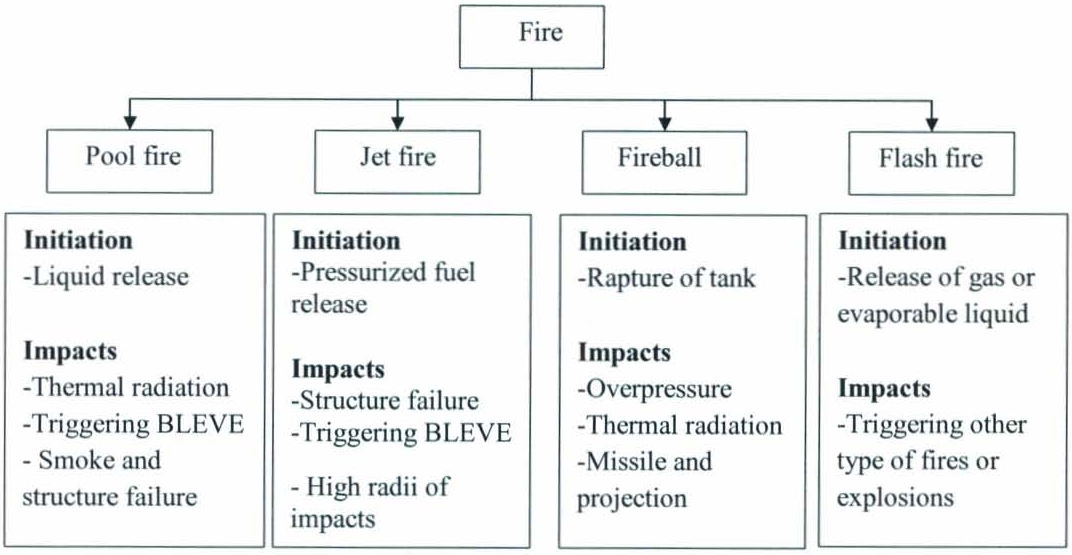

Figure 4.1: Different fire categories and their hazards.

4.2 Modeling

After understanding of the scenario's requirements, specifications and characteristics, mathematical modeling is used to estimate the possible scenario consequences. A variety of tools and models are available to perform consequence assessment. Selecting the optimal model requires an understanding of their strength and limitations.

4.3 Models

In fire modeling the objective is to understand fire behavior and its outcomes. Depending on required accuracy, complexity of system and required time there are numerous mathematical models which could be used for fire modeling. Based on the employed mathematical techniques

and solution methods, mathematical models can be divided in three main categories: empirical correlations, zone models and CFD models.

4.3.1 Empirical Correlations

Empirical correlations based models are the simplest models. They are based on empirical relations which have been developed considering the algebraic relation between input parameters and outcomes of fires. Since in fire modeling especially in open area thermal radiation and convection are the most important parameters, these models are mostly devoted to estimate thermal radiation, temperature profile and convection. For example in jet fire modeling, parameters like type of fuel, fuel mass rate and discharge diameter is used to estimate thermal radiation, convection and the visible length of the flame.

Although these models are fast and user friendly, there are several limitations which restricting their application. First of all, most of these models are on the base of finite number of experiments constrained with experimental conditions. Secondly, there are inherent error associate with fitting correlations to a restricted data set. Furthermore, most of the experiments have been carried out for open spaces or very simple and not congested enclosures. So these models may not be applied for highly congested workplaces like offshore structures.

4.3.2 Zone Models

The application of zone models started in mid-1950 with introduction of one zone models for study of post-flashover and specially movement of toxic gases in other compartments. Later two zone models were developed for pre-flashover behavior estimations. The concept behind zone models is to divide compartments or enclosures into two or more spatially homogenous volumes (zones). The model has been observed to take place in real cases and experiments [15, 16]. In

these models, the upper layer has higher temperature and temperature drops in subsequent lower layers. In these models, the plume concept is used to take into account smoke and hot air movement above the fire.

For each spatial volume (zone), physical parameters such as species concentration, temperature and density are assumed to be uniform. This means that all the particles in a specific zone have same properties and these properties change only with time. Although the results from experiments show some perturbations and variations from these assumptions, in general the results of these models are in good agreement with experiments.

Mass, momentum and energy conservation equations result in a set of Ordinary Differential Equations (ODE). The conservation equations are coupled with gas laws (typically the ideal gas assumption) for calculations. In zone models the physical properties in a zone considered homogenous; thus, conservation laws are applied to estimate energy, mass and momentum transport between adjacent zones. Calculations are conducted by modeling sub-fire processes: convection, diffusion, combustion and fluid flow.

The momentum conservation law is not applied explicitly as not all the required information for pressure and velocity is available in the model. The application of momentum conservation law is governed by the mass movement from plume fire to zones and from adjacent zones to ventilation and open areas.

Zone models maybe classified based on the number of zones in each compartment: one zone, two zone and multi zone models. In one zone models the entire compartment has the same properties like temperature and species concentration. Due to plume rising and fire turbulent behavior, these types of models are not appropriate where there is a fire. Such a one zone model

has been developed and used for analysis and estimation of smoke movement in other compartments.

Two zone models divide the volume of enclosure to two volumes where the upper zone is at high temperature and the lower zone at lower temperature. This layering is due to buoyancy effect and the rise of hot gases from plume. These models are more realistic in comparison to one zone models even when only the smoke movement in remote compartments is studied. This is due to presence of colder air in remote compartment, buoyancy effect and finally stratification. Because of two zone model abilities, they could be used for pre-flashover and post-flashover fire modeling. Figure 4.2 presents control volumes for two zone models.

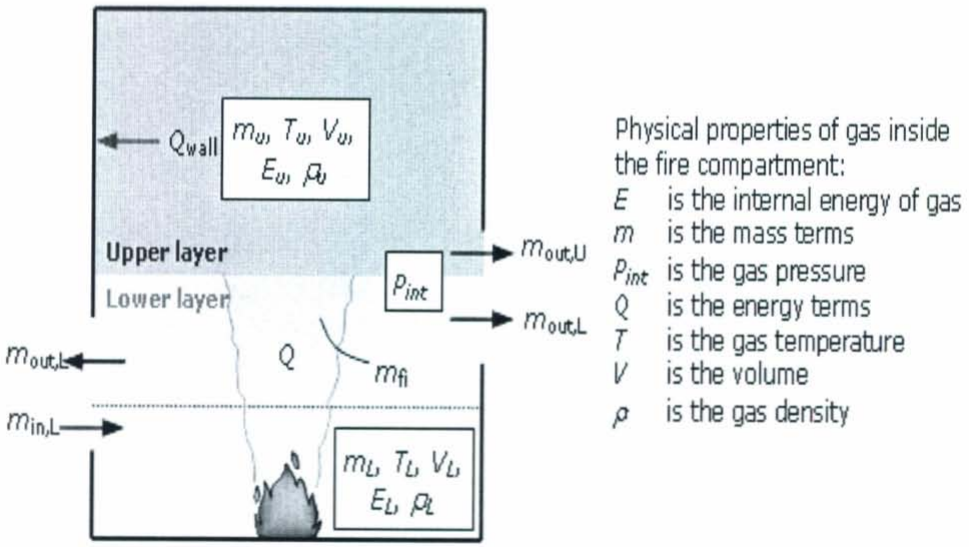

Figure 4.2: Control volumes and zones for a two zone model. Retrieved 12 January 2011 from:http://www.mace.manchester.ac.uk/project/research/structures/strucfire/Design/performance/fireModelling/zoneModels/twoZoneModel.htm

Finally multi zone models were developed to improve accuracy and also predict vertical temperature variations and toxic gas concentrations [17, 18]. In this method, the compartment space is divided into an arbitrary number of zones and the physical properties of each layer are assumed to be uniform. The fire plume flow does not mix with adjacent layers and fire plume flow is upward until it reaches the ceiling. Therefore, in these models the assumption is that all the heat is transferred to the top layer.

Conservations laws are solved in the boundary of layers to estimate the average values of parameters such as temperature in layers. Due to the presence of multiple zones, computational time is longer than two zone models. Figure 4.3 shows segments of a multi zone model.

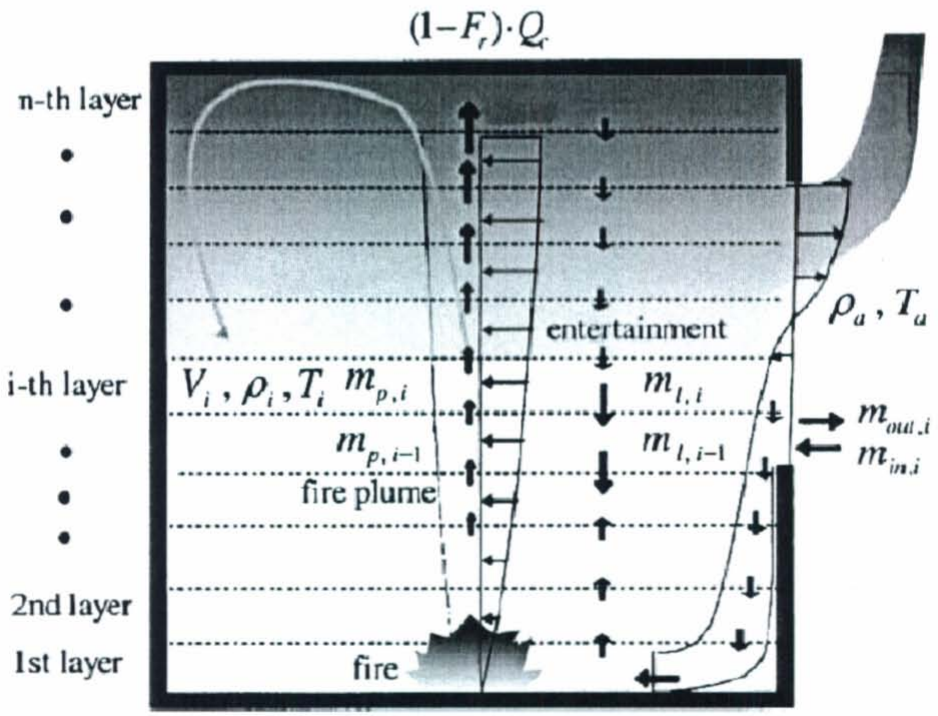

Figure 4.3: Layers of a multi zone model.

Although different zone models apply different methodology and techniques for calculations, they have some assumptions in common which distinguish them from CFD models:

- Uniform physical properties inside each zone.
- No diffusion between zones boundaries.
- Diffusion can occur between zones and the enclosure wall. Although in most modeled it is neglected (due to very small value).
- Plume flow rises to the ceiling continuously.
- Plume flow does not mix or affect moderate level zones in its rising.
- In most of models, the horizontal cross section (area) of the compartment is constant.

Numerous zone models have been developed and validated with experimental results. The below table presents most commonly used models.

Table 4.1: List of zone models with a brief description [19, 20].

Model	Country	Description
ARGOS	Denmark	Multi-compartment zone model
ASET	US	One room zone, no ventilation
ASET-B	US	ASET in BASIC language instead of FORTRAN language
BRANZFIRE	New Zealand	Multi room zone model, including flame speed, multi fire and mechanical ventilation
BRI-2	Japan/US	Two layer zone model for multistory, multi compartment smoke transport
CALTECH	US	Pre-flashover zone model
CCFM.VENTS	US	Multi room zone with ventilation
CFIRE-X	Germany	Compartment fire, specially liquid hydrocarbon pool fire
CiFi	France	Multi room zone model
COMPBRN-III	US	Compartment zone fire
FFM	US	Pre-flashover zone model
FIRAC	US	Include complex vent systems

FIREWIND	Australia	Multi room zone model with several smaller sub-model
MRFC	Germany	Multi room zone model for smoke movement and temperature load on structures
NAT	France	Single compartment zone model with attention to response of structures
OZONE	Belgium	Zone model with attention to structure response
RFIRES	US	Pre-flashover zone model
SFIRE-4	Sweden	Post-flashover zone model
WPIFIRE	US	Multi room zone fire

4.3.3 Zone Models Limitations

Zone models are limited due to assumptions during derivation, formulation and application. One of the most important assumptions in these models is that a compartment is to be divided into small number of uniformed property zones and calculations are to be done with in each layer. Since in each layer all the physical properties are the same, there is no temperature or concentration gradients in the layer. This means that in whole layer, temperature and gas concentration is the same regardless to the location of fire or vent. This is problematic when the gas concentration or temperature at a specific location is critical, for example when determining the optimal location of smoke detectors.

The other limitation is due to zone transparency and radiation. The radiation magnitude is directly a function of surrounding environment: species concentration, absorption coefficient and temperature. The assumption of a uniform hot layer above the cold layer overestimates radiative heat from hot layer to cold layer. This in turn could result in underestimating the temperature of the hot layer.

One of the main shortcomings of zone models is the inability to account for turbulent plume behavior. Especially in multi zone models where there are several layers, the assumption that hot

gases move upward towards the ceiling without any effect on intermediate layers. This result in an underestimation for lower layers temperatures and overestimation for upper layers temperature.

Most of zone models need the rate of heat release before starting the simulation process. The rate of heat release is a function of combustion efficiency which in turn is related to air to fuel rates. For example when oxygen concentration decreases, for a solid fuel, flame length may decrease and change to a smoldering process. Since the heat release rate changes with time and space, using it as an input parameter will impact the model accuracy.

4.3.4 Computational Fluid Dynamic (CFD) Models

Rapid growth of both hardware and software computer knowledge and technology have moved models from correlation based to compute based on the governing equations (CFD models). Although description of CFD is behind the scope of this thesis, a brief description is helpful. A CFD model is a deterministic tool for simulating real time scenarios. CFD models approximate the solution of a set of algebraic and differential equations. However here, equations are solved based on local approximation of differential equations.

In these models a set of non-linear, time and spatial dependent equations (Navier-Stokes) are solved over the domain of interest. These models can capture turbulence through introduction of turbulent equations. The way in which turbulence is taken into account is important; basically CFD models are classified base on the method of describing turbulent.

Turbulence is a state of flow motion that involves three dimensional random vortices, higher energy dissipation, mixing and drag effects. CFD models have different methods for turbulent modeling: Reynolds Averaged Navier-Stokes (RANS), Large Eddy Simulation (LES), Direct

Numerical Simulation (DNS), Detached Eddy Simulation (DES) and Turbulence near wall modeling. The first and second methods are the most popular, applicable and frequency used.

It is not surprising that the DNS is the most accurate model [21-24]. The DNS model was introduced in 1970 to model isentropic turbulence up to Re = 35. This model solves Navier-Stokes equations in a very fine grid and a very small time steps to capture the turbulence, vortex and fluctuations. The reason why DNS models are not used in most of engineering applications is due to their very long computational requirement time. Furthermore, DNS are needed to be solved in three dimensional spaces where turbulence and vortices exist. Because of these limitations, DNS are mostly used as a research tool to understand the fundamental turbulence behavior and are used to calibrate other available models like RANSs and LESs.

The purpose of RANS is to estimate Reynolds stresses. This may be done by three different methods: Linear Eddy Viscosity models, Nonlinear Eddy Viscosity models and Reynolds Stress models (RSM). In linear eddy viscosity models, the Reynolds stress is modeled through introducing a linear constitutive relationship with main flow strain field. However, linear eddy viscosity models are known to fail in a number of flow situations. For example these models over-predict turbulence energy level in stagnant regions. Moreover these models usually over-predict K (Kinematic energy) near the walls where actually K can be neglected. Because of these shortcomings, at present, linear eddy viscosity models are rapidly replaced by nonlinear eddy viscosity models in engineering applications.

With respect to accuracy and complexity, LES lies between RANS and DNS models. In this model, small eddies are removed and modeled by Sub-Grid-Scale (SGS) models. Kolmogrov's theory (self-similarity theory) states in turbulent flow large eddies are dependent on geometry

while small eddies are universal which allows for an explicit solution of large eddies and implicit solution of small eddies by SGS models. This filtration enables higher Reynolds number (more turbulent flows) to be modeled. However this filtration may result in lower accuracy especially near wall boundaries. To compensate this situation, a much finer mesh is required.

For most of engineering applications the accuracy of RANS models is sufficient. Recently hybrid models have been introduced. These models are a combination of LES and RANS methods. These models have the advantages of both categories of models: speed of RANS and accuracy of LES.

4.3.5 CFD Models Requirement

Lots of engineering problems are addressed by CFD models; however, for fire modeling applications, a model should have certain features to be used. Turbulence modeling is one of the most important features. This is more important for jet fire modeling since the flow is highly turbulent. One other important criterion is heat release and radiation modeling. Inefficient modeling of soot may result in completely different outputs; thus, especial treatment of soot particles is mandatory. Combustion modeling is of importance due to its direct effects on combustion process outputs such as heat release and smoke. Boundary and initial condition are employed to obtain unique solution. Beside all of these, a model should be able to intake complex geometries without restrictions on space or time steps.

Fires and especially jet fires are highly turbulence phenomena. After the combustion process, numerous eddies in variable sizes are generated. While initially eddies are on large size, they breakdown into smaller eddies and vortices as the initial energy dissipates. To take into account such behaviors, the turbulence model plays a critical rule. Most of CFD tools employ

RANS turbulence modeling (especially K-ε and K-ω). Results are reliable and less computational time is required in comparison to LES based CFD models. For more congested areas like engine rooms, due to high turbulence flow in the case of fire, LES based models may be used.

In general radiation modeling of a liquid fuel fire is easier than gas fuel fires because gas fuel fires more complex, turbulent and unpredictable. The radiation equation is a combination of integral and differential terms (integro-differential equation) which makes solving more difficult. Radiation depends on parameters like temperature and composition; therefore, to solve radiation equation, assumptions for radiative properties of medium are needed. Typical models for radiation modeling are point source and solid frame models. In point source models, the total released heat of fire and fraction which is converted to radiation are required. Point source models are accurate for far distances but over-predict for near distances due to the fact that the thermal radiation is emitted from a single point. In contrast, in solid frame models heat is emitted from an idealized shape (e.g. cone or cylinder). Although this model is simple, it requires the estimation of flame height and diameter. In conventional solid frame models, all the height of flame was considered to participate in radiation. However modified solid flame models has been developed that only the luminous flame zone participates in calculations.

Where in models such as ISIS-3D, the only flame edge zone radiates and hot gases and soot outside the flame do not contribute in the radiation. ISIS-3D is able to accurately calculate the characteristics of engulfed objects and has a relatively short computational time. This assumption may result in under-prediction of radiation calculations and heat load on human or structure due the neglecting of hot gases radiation above the flame.

Other models may employ different radiation transport algorithms like ray tracing. This is a simple method which uses randomly generated rays between source and targets to represent the radiation phenomenon. Such a simple model is not able to represent the effect of surrounding environment and the effects of hot gases, walls and equipment are neglected in such models.

Another more advanced models to handle radiation are Radiative Transport Equation (RTE) models. Although in practical simulations this model cannot be solved accurately, the accuracy is much better than ray tracing, point source and solid frame models. RTE models estimate radiation intensity based on wavelength banding. Here, the radiation spectrum is divided to small number of bands and a separate RTE is solved for each band. The whole intensity is obtained by summation of all bands; as the number of bands increases, accuracy increases and also the computational time increases. In this model, the limits of bands are selected carefully to represent the most important radiation bands of important components, mostly CO_2 and H_2O. Finally it should be noted that radiation fraction in real fire scenarios depends on fuel type, soot and oxygen concentration and temperature. Hence, using a constant value (default value of tool) causes error and deviation in calculations.

Combustion is the process in which species are formed and destroyed by chemical reaction. For most of cases which have been discussed in this thesis, combustion is non-premixed phenomenon like a jet fire, pool fire or fire ball. Combustion consists of two coupled phenomena: thermal and chemical. The chemistry of combustion is highly exothermic (high release rate of heat). Therefore combustion is a self-accelerating process, in most models is considered as an irreversible phenomenon. The chemical reactions are dependent on the type of fuel. This is even more complex when the fuel is in a liquid phase which needs to evaporate, diffuse and finally react. Combustion of fuels results in generation of numerous products from

stable compounds to less stable radicals. To simplify the combustion process, the only major products (stable) are considered; CO_2, H_2O and CO. The classical approach for combustion modeling is based on probability density functions which allow the determination of mean reaction rate. A more advanced representation of combustion relies on Flamelet concept.

To uniquely define a problem using CFD, a set of boundary and initial values are needed. Boundary conditions specify the limitations on the space and initial values define properties in the beginning of simulation. Generally there are two types of boundary conditions: thermal and velocity. Thermal boundary conditions include constant temperature where the temperature of wall assumed constant, adiabatic where a zero heat flux is assumed. Other boundary conditions like constant heat flux may be used also. Setting the appropriate thermal boundary condition is important since it directly affects the temperature profile, smoke behavior and final consequence. Velocity boundary conditions include as no slip, slip, no penetration and penetration boundaries.

All CFD models discretize time and space into finite number of meshes and estimate parameters in the center or edges of meshes. The accuracy of approximation depends on the size of meshes and to a certain level, as mesh is finer, the result is more accurate. Therefore, to obtain accurate results, users may need to reduce the size of meshes and time steps. As the number of meshes increases, computational time increases as well. Space discretizing must be based on the geometry and complexity of scenario. While most of tools usually apply a Cartesian discretization, radial is required in some geometries. More advanced tools may use body fitted coordinate (BFC): as the object deforms, the grid deform. Application of BFC improves the accuracy and may save computational time since the only part which is needed is calculated.

Table 4.2 shows the most commonly used CFD tools and a brief description. It is user responsibility to comprehensively be familiar with a tool, be aware of assumptions and limitations.

Table 4.2: CFD models for fire modeling applications.

Model	Country	Description
ALOFT-FT	US	Smoke movement from large out-door fires
CFX	UK/US	Applicable to fire and explosion
FDS	US	Smoke and hot flow movement, response of sprinklers
FIRE	Australia	Capable of modeling water spray
FLACS	US	Fire and explosion modeling
FLOW3D		Solving convection equations
FLUENT/AirPak	US	Flow with heat transfer and reactions
JASMINE	UK	Smoke movement
KAMELEON	Norway	Thermal response of structure
KOBRA-3D	Germany	Smoke movement and heat transfer
MEFE	Portugal	Smoke movement into one or two Compartments
OpenFoam	UK	General purpose code, open source Adaptable for numerous applications
PHOENICS	UK	General purpose CFD code
RMFIRE	Canada	Transient smoke movement
SMARTFIRE	UK	Spread of fire hazards inside enclosure
SOFIE	US/Sweden	Contains sub-models for different Applications
SOLVENT	US	Smoke and heat transfer
SPLASH	UK	Interaction of hot gases with sprinkler spray
STAR-CD	UK	General purpose tool
UNDSAFE	US/Japan	Open fire or inside enclosure

4.3.6 CDF Models Limitations

The most significant limitation in CFD modeling is computational time. Detailed modeling may take from hours to days depending on the complexity of geometry and used software. Moreover, some limitations are related to the methodology which has been applied. For example,

UNDSAFE has been developed based on a finite difference scheme. Thus, this model has an inherent difficulty for complex geometries.

Sub-models which have been used in a model usually have limitations and affect the results. For example if a thermal element sub-model has been used for combustion modeling, the outcome is significantly different from a Flamelet sub-model. The complexity of the combustion process has a direct effect on both results and computational time. Species considered in the simulation impact radiation and calculated heat load on the structure. Furthermore, the general technique for turbulence modeling results in diverse outcomes. Determination on if a boundary has a constant temperature or a constant heat flux is a complicated task. For example in fire modeling inside an enclosure, the wall may show constant heat flux at the beginning and then switch into a constant temperature boundary as the temperature increases. This is more complicated when the properties of wall and its behavior is not known completely. The other limitation may arise due to required data and training. Some software needs special training to acquire the ability to work with its sub-models, inter-connection of sub-models and obtain reasonable results.

The main limitation emerges when the appropriate sub-models to simulate the specifications are not present. For instant, snow and ice have great capacity to absorb convectional heat and reflect radiation. Thus melting and evaporation of snow/ice have significant effects on the near field due to heat absorption. The presence of more vapors in the near field affects the concentration of species, stoichiometry of reactions, hot gases heat capacity and radiation parameters of media. For far field, there are opposing factors: snow/ice refection may increase the radiation intensity, however, transparency of the near field air, and radiation index of fire may have decreased due to presence of more vapor and less temperature.

4.4 CFD Models versus Zone Models

Zone models were developed and used to investigate the fire and smoke behavior inside an enclosure. In these models whole compartment is divided into two or more zones and average parameters calculated for each zone. As the number of zones increases, the results improve if geometry is simple. However, as the geometry becomes more complex, the accuracy is lost. In contrast, CFD models are able to take into account more details and the solution changes based on the variation of detail inputted. This generality and adaptation for different cases and scenarios make CFDs as very useful tools [25]. Moreover, the application domain for zone models is limited to compartments where dividing of space into several separate volumes could be done. In contrast CFD models could be applied to open spaces.

Zone models are easy to learn and also required very short computational time in comparison to CFD models. Zone models are effective when the objective is the understanding of phenomena, and general behavior. Thus, they may be applied for quick approximation and in the beginning of design. In contrast, CFD models require long computational time and thus could be used in the final steps of design: when detailed design is needed. Table 4.3 compares Zone and CFD models.

Table 4.3: Comparison between Zone models and CFD models.

Criteria	Zone Models	CFD Models
Accuracy	Acceptable for some engineering applications, depending on the sub-model -s and zone boundaries.	Depending on the resolution of mesh, turbulence modeling and sub-models; more accurate than Zone models.
Applications	Indoor fire behavior and smoke movement, suitable for preliminary calculations when just a general behavior is required	Indoor and outdoor fire behavior and smoke movement. Fire spread and structure response. Detailed analysis, sensitivity and optimization of design.
Computational	Short time, is suitable when	Long computational time, depends on

time	several modeling is required to compare general behavior of different situations	the required accuracy and geometry. For complex geometries several hours to days are required.
Input data	Depending on the model and its sub-models, generally height of ceiling, heat release rate, fire height, heat loss factor and etc.	Setting boundary conditions, providing sub models inputs and meshing,
Limitations	Applicable for simple compar-tments, fire position does not considered in calculations, not vertical variation in the results	Long computational time, sub-models lack,
Operation knowledge	Relatively easy to acquire operation skills, define zones, input sensible heat release rate and etc.	Some software need special training, preparing each scenario may take a long time as well
Output data	Average concentration and temperature in the zones,	Temperature and concentration in each grid, structure response

Chapter 5: Modeling of Pool Fires in Arctic Region

In the previous chapter, different types of fires and modeling method were discussed. Fires and especially pool fires are among the most frequent accidents in process facilities. Flame impingement and thermal radiation are the main hazardous characteristic of pool fires. Pool fires have been the subject of numerous modelings and experiment studies covering verity of areas such as fire and flame structure, emissivity power, temperature distribution and fire distinction. The effects of environmental parameters such as wind velocity, humidity and water/ice droplets in the air have not been studied extensively. Further, the effect of surrounding surface reflectivity has not been studied. This issue is very important for cold regions like the arctic where outdoor surfaces are covered with snow and ice for several months of the year. Furthermore, there is no comprehensive fire consequence modeling tool that includes pool fire development, environmental characteristics effects and thermal radiation. This study proposes a new comprehensive model for steady state and fully developed pool fire. This new model takes into account the effects of environmental variables such as temperature, the presence of droplets and surface reflexivity on the thermal radiation and subsequently on the fire consequence assessment.

5.1 Previous Works

In storage facilities, the design and implement of surrounding systems which collect and drain accidental released liquid hydrocarbon is a usual practice [26]. Ignition of the collected and drained liquid results in a pool fire. A pool fire is defined as a turbulence diffusion flame controlled by buoyancy forces [27-29]. Here the combustion phenomenon is characterized by low momentum diffusion flames. A pool fire is divided into three different regions: flame base

(persistent zone), intermittent zone and finally plume zone [28-30]. The persistent region is rich in flammable vapors and flow is laminar and as a result it maintains its shape and structure. The intermittent zone is characterized with fluctuating and turbulent flame and flow. In this zone, fuel vapors are consumed completely and due to turbulence, the temperature and radiation are higher compared to the persistent zone [31]. In the plume zone no reaction occurs, Turbulent flow and smoke characterize the zone. Due to presence of smoke and soot, radiation level is lower.

The behavior of a pool fire is tightly bound to the pool size [32]. The size of pool controls the height of different zones, thermal radiation and temperature; therefore, extrapolation of these parameters may result into large errors. Temperature, thermal radiation and duration are the most important parameters in consequence assessment of pool fire [33]. Depending of these parameters, consequence of fire may be immediate (e.g. the personals are exposed to radiation) or delayed (e.g. heating up the structures and domino effects). The hazards associated with pool fires are related to the thermal radiation [34]. The thermal radiation depends on the type of fuel, soot yield and flame temperatures [35]. Numerous studies have been conducted to investigate the radiation phenomenon of pool fires. Modak [36] presented a theoretical study for thermal radiation of horizontal and axisymmetric pool fires. Orloff [37] introduced a simple model to calculate the radiation of pool fires by simplifying non-homogenous and non-isothermal fires to equivalent isothermal and homogenous fires. Hamins et al. [38] conducted a set of experiments for different fuels to develop and modify methodologies for thermal radiation measurements. Later, Rew et al. [28] proposed a semi-empirical correlation for thermal radiation of hydrocarbon pool fires. Chun et al. [34] have conducted both experiments and CFD simulation to study radiation of pool fires. Jensen et al. [35] and Krishnamoorthy [39] studied different approaches to radiation modeling, effects of soot and smoke effects on the estimated radiation level. However,

environmental variables like surface reflexivity or the presence of water/ice droplets were not included in these studies.

Kim et al. [40] experimentally investigated variables such as the effects of direct-downward water/ice spray on the burning rate, behavior and extinction of pool fires. They have reported that small water/ice droplets are ineffective and may inversely increase the burning rate. Later studies suggested that direct-downward spray is not the optimum direction and the efficiency of extinction increases as spray direction goes toward horizontal [41]. Chen et al. [42] studied the effect of initial fuel temperature on the burning rate and burning states of pool fires. Their experimental study shows that the duration of steady burning decreases as initial temperature of fuel increases. Furthermore, if initial fuel temperature reaches the boiling temperature, there would not be steady burning period. Ravigururajan [43] has proposed a method to calculate the effect of water/ice droplets on the thermal radiation attenuation.

Despite numerous works investigating pool fires, the effect of environmental variables has not been comprehensively studied. In most of studies just a single environmental parameter has been considered. The combination of these environmental variables will affect the consequence of any pool fire especially in arctic region as these parameters coexist and affect the behavior and thermal radiation of pool fire. In this study a new model is developed which takes into account environmental parameters including temperature, wind, the presence of droplets and surface reflectivity. The Fay model [33] was used as the base for the model. This model has the advantage of a continuous temperature distribution. Furthermore, it also includes the effect of water/ice droplets and surface reflexivity. Therefore, the proposed model accounts for all environmental variables related to the Arctic.

5.2 Pool Fire Modeling

The flame of pool fires is typically nonuniform in temperature and species concentration distribution in terms of three dimensional calculations; therefore, modeling of pool fires is challenging. Pool fire models are generally classified into two groups. The simplest model assumes thermal radiation controls fuel evaporation. These models do not account for combustion and air entrainment in their calculations rather calculating radiation based on flame temperature, size and shape. Orloff [37] presented such a model to calculate the radiation of pool fires. In contrast to simple models, fundamental models prescribe the fire behavior based on air entrainment, mixing, combustion, flow and plume rising. Fay [33] has recently proposed such a model for a wide variety of pool sizes and wind velocities.

5.2.1 The Fay Model

This model is a two zone pool fire model which describes flame properties, combustion and plume zones. The combustion zone begins from the base of fire and goes up to the end of visible flame. In this zone the evaporated fuel vapor reacts with air in stoichiometric proportions and forms combustion products. When fuel evaporates from pool surface, it enters a circulation region. Fuel vapor flows radially toward the edges of pool fire; then, moves upward and inward toward the flame tilt in the center line. A portion of fuel vapor moves downward toward the liquid surface and hence the circulation is completed. This fuel circulation provides fuel vapor for flame surface. Fuel vapor and air diffuse respectively outward and inward and intersect each other on flame surface where reaction occurs and heat is released. The released heat results into temperature increase and density reduction and subsequently upward diffusion and bulk movement of products. The low density and high temperature products enter plume zone. The

plume zone is above combustion zone and rises until temperature significantly decreases and product gases dilutes.

Temperature and fuel concentration distribution are functions of the mixing process. If mixing is diffusion driven and laminar, oxygen and fuel vapor diffuse and reaction occurs. For this case, the flame surface is thin and temperature is almost equal to adiabatic flame temperature. Since the phenomenon is laminar, the changes of temperature and combustion products concentration is sudden where both temperature and combustion products concentration increase rapidly in a thin layer. In contrast to laminar and diffusive flames, the rapid mixing ensures the temperature change is smooth due to turbulence. Hence the flame surface temperature is less and flame surface thickness is greater compared to the laminar regime. Taking a horizontal plane with cross section A at a height z above pool fire and considering the vertical velocity to be equal to ω; mass (M), momentum (P) and energy (E) can be written as

$$M = \int_0^A \rho\omega \, dA \tag{1}$$

$$P = \int_0^A (\rho\omega)\, \omega \, dA \tag{2}$$

$$E = \int_0^A (\rho\omega) C_p \, (T - T_a) dA = C_p T \int_0^A \omega(\rho_a - \rho) dA \tag{3}$$

Where, C_p, ρ and ρ_a are constant specific heat, flow density and ambient air density respectively. Mass flux growth depends on the air entrainment which is related to diameter and height of combustion and plume zones. Hence mass flux variations for these zones may be shown by Eqs. (4 and 5) respectively.

$$\frac{dM}{dz} = \alpha_c \left(\frac{\rho_a P}{M}\right) D \tag{4}$$

$$\frac{dM}{dz} = \alpha_p \sqrt{\rho_a P} \tag{5}$$

Where α_c and α_p are dimensionless constants for combustion and plume zone respectively and D is the pool diameter. Eq. (4) shows that the rate of mass flux growth decreases rapidly as mass flux increases in combustion zone. In contrast, mass flux growth is just explicitly proportional to momentum in the plume zone. Due to buoyant force and growth of mass flux, it is expected that vertical momentum increases with height as shown by Eqs. (6 and 7) for combustion and plume zones respectively.

$$\frac{dP}{dz} = \int_0^A g\,(\rho_a - \rho)\,dA = \eta_c \left(\frac{g}{C_p T_a}\right)\left(\frac{EM}{P}\right) \tag{6}$$

$$\frac{dP}{dz} = \int_0^A g\,(\rho_a - \rho)\,dA = \eta_p \left(\frac{g}{C_p T_a}\right)\left(\frac{EM}{P}\right) \tag{7}$$

Where, η_c and η_p are dimensionless constants. These equations are similar and only vary in their constants. Finally variation of energy with height can be shown by Eqs. (8 and 9) for combustion and plume zones respectively.

$$\frac{dE}{dz} = \emptyset_c \left(\frac{h_c}{f}\right)\frac{dM}{dz} \tag{8}$$

$$E_p = h_c \left(\frac{\pi D^2}{4}\right) = \left(\frac{\pi}{4}\right) h_c \rho_a g^{0.5} D^{2.5} F_t \tag{9}$$

Where, h_c, f, $\dot{m}$ and $\emptyset_c$ are fuel heating value per mass of fuel, mass ratio of products to fuel in a stoichiometric mixture, fuel burning rate per unit and the combustion zone equivalence ratio.

Eq. (9) shows that energy is constant in plume zone and is directly related to pool fire burning rate. In this equation, F_t represents the fuel Froude number and is shown as

$$F_t \equiv \frac{}{\rho_a \sqrt{gD}} \tag{10}$$

In the integration of Eqs. (4, 6 and 8), it has been assumed that mass flux, momentum and energy are zero at the base of pool fire. This assumption is valid since released energy and vertical velocity are very small in the base of fire compared to the top of combustion zone. Integrated form of mass, momentum and energy equations in the combustion zone are

$$M_c = \alpha_c \rho_a D \left[\frac{2}{9} \left(\frac{\eta_c \emptyset_c}{\alpha_c}\right)\left(\frac{h_c}{f C_p T_a}\right)\right]^{0.5} g^{0.5} z^{1.5} \tag{11}$$

$$P_c = \frac{3}{4} \left(\frac{\eta_c \emptyset_c}{\alpha_c}\right)\left(\frac{h_c}{f C_p T_a}\right)\left(\frac{g {M_c}^4}{\rho_a D}\right)^{0.33} \tag{12}$$

$$E_c = \emptyset_c \left(\frac{h_c}{f}\right) M_c \tag{13}$$

P_c and E_c in Eqs. (12 and 13) are functions of M_c, however, the scaling relation for P_c and E_c versus z can be found to be 2 and 1.5 respectively. Based on Eqs. (11-13), average vertical velocity and temperature are estimated as

$$\omega^{`}_c \equiv \frac{P_c}{M_c} = \left[\frac{1}{2} \eta_c \emptyset_c \left(\frac{h_c}{f C_p T_a}\right) g z\right]^{0.5} \tag{14}$$

$$T^{`}_c - T_a \equiv \frac{E_c}{C_p M_c} = \frac{\emptyset_c h_c}{f C_p} \tag{15}$$

Where, $\omega^{\cdot}_{c}$ and $T^{\cdot}_{c}$ are average temperature and vertical velocity in combustion zone. While $\omega^{\cdot}_{c}$ is proportional to $z^{0.5}$, $T^{\cdot}_{c}$ is independent of z in combustion zone and is constant. Flow area at any height is obtained using:

$$A_c \equiv \frac{M_c}{\rho_a \dot{c}} = \frac{2}{3}\alpha_c{}^{0.5} Dz \tag{16}$$

Finally the height of combustion zone can be obtained replacing $E = E_p$ at $z=L_c$ as

$$\frac{L_c}{D} = \frac{f}{\emptyset_c}\left[\frac{9\,\pi^2 C_p T_a}{32\eta_c \alpha_c h_c} F_t{}^2\right]^{0.33} \tag{17}$$

For the plume zone, Eqs. (5 and 7) are integrated to achieve mass flux, momentum and energy relations respectively. To integrate and solve these equations, initial condition cab be set equal to values at the end of combustion zone. This results in a new set of unknown coefficients. The alternative method is to introduce an imaginary source at z_0 below the pool fire and find the plume solution for this location. This initial condition results into discontinuity of solution at $Z=L_c$, this is the only practical method to get reasonable equations and results. Eqs. (18 and 19) present the integrated form for mass flux and momentum in plume zone, respectively.

$$M_p = \left[\frac{243}{2500}\frac{\eta_p \rho_a{}^2 E_p \alpha_p{}^4}{C_p T_a}\right]^{0.33} (z + z_0)^{1.66} \tag{18}$$

$$P_p = \left[\frac{5\eta_p E_p}{4\alpha_p C_p T_a \sqrt{\rho_a}}\right]^{0.4} M_p{}^{0.8} \tag{19}$$

Based on these equations average velocity, temperature and area of the plume zone are obtained as:

$$\omega^{\cdot}_{p} \equiv \frac{P_p}{M_p} = \left[\frac{25\,\pi\eta_p h_c F_t D}{48\alpha_p{}^2 C_p T_a (z+z_0)}\right]^{0.33}\sqrt{gD} \tag{20}$$

$$T^{\cdot}_{p} - T_a \equiv \frac{E_p}{M_p C_p} = \left[\frac{625\,\pi^2 T_a}{732}\left(\frac{h_c F_t}{C_p T_a \alpha_p \sqrt{\eta_p}}\right)^2\left(\frac{D}{(z+z_0)}\right)^5\right]^{0.33} \tag{21}$$

$$A_p \equiv \frac{M_p}{\rho_a \dot{}_p} = \alpha_p\left(\frac{3}{5}\right)(z+z_0)^2 \tag{22}$$

These set of equations reveal that temperature decreases rapidly in the plume zone as plume area increases due to air entrainment. To complete the above equations, a formula which relates mass burning rate to the fire and fuel characteristics is need. The fuel burning rate has been used in the fuel Froude number. Fay presented a set of simple equations for two different cases. If the thermal radiation is small compared to heat convection, then the burning rate can be expressed Type equation here.as:

$$\dot{m} = (1 \pm 0.19)1.30 \times 10^{-3}\left(\frac{\rho_a\sqrt{gD}h_c}{h_v(1+f)}\right) \tag{23}$$

Where, h_v and h_c are heat of evaporation and fuel heating value respectively. (±) shows the uncertainty of using these equations. For large pool fires which are usually turbulent, radiation is the main mechanism of heat transfer from flame and hot gases into the liquid surface. The burning rate can be expressed as Eq. (24) under these conditions.

$$\dot{m} = 1.0 \times 10^{-3}\left(\frac{h_c}{h_v}\right) \tag{24}$$

Unit of the burning rate is (kg/m^2s) in Eqs. (23 and 24). When pool fire characteristics like flame temperature, diameter, burning rate, visible height are known, the thermal radiation of the

pool fire can be simulated. Gray gas model [17] and surface emissive power are the most widely used models. Fay has used a gray gas sub-model in his pool fire model. The main assumption in this model is that soot concentration is proportional to the local concentration of products.

For large pool fires, due to significant generated soots, only the base of fire may be assumed to contribute into thermal radiation. The height of this region is inversely proportional to soot emissivity (k). Considering a cylindrical and untilted fire, the thermal flux to a receiver at distance x from the edge of a pool fire can be calculated as

$$q = \gamma\sigma {T_f}^4 \frac{x}{\pi y}\left(\frac{2}{\sqrt{y^2-1}}+\frac{y^2+1}{y^2-1}\arctan\sqrt{\frac{y+1}{y-1}}-\arctan\sqrt{\frac{y-1}{y+1}}\right) \quad (25)$$

Where,

$$x \equiv \frac{1}{kR}; \quad y \equiv 1+\frac{x}{R}; \quad R \equiv \frac{D}{2} \quad (26)$$

Atmospheric instability has been considered by including a crosswind sub-model. Although the cross wind usually does not change the size of visible flame, it causes the flame to tilt through an angle θ from the vertical axis. Therefore in the case of wind the height of visible flame can be calculated

$$H_v = L_v \cos(\theta) \quad (27)$$

The other issue related to crosswind is the increase of air entrainment. These variations include both vertical and horizontal motions of the plume gas with respect to the crosswind. Therefore, mass flux and momentum for the plume zone can be rewritten as

$$\frac{dM}{ds} = \alpha_p\sqrt{\rho_a P} + V\left(\frac{M}{\sqrt{\rho_a P}}\right)(\beta_v \cos(\theta) - \beta_h \sin(\theta)) \quad (28)$$

$$\frac{dP}{ds} = \eta_p \left(\frac{g}{C_p T_a}\right)\left(\frac{E_p M}{P}\right)\cos(\theta) + V\sin(\theta)\left(\frac{dM}{ds}\right) \quad (29)$$

Where, s is the centerline of the plume. For the case of axisymmetric plumes, the values of β_v and β_h have been reported to be 0.5 and 0.1 respectively [24]. By integrating Eqs. (28 and 29) new equations for the plume zone can be obtained. Figure 5.1 presents the solution steps of the Fay model.

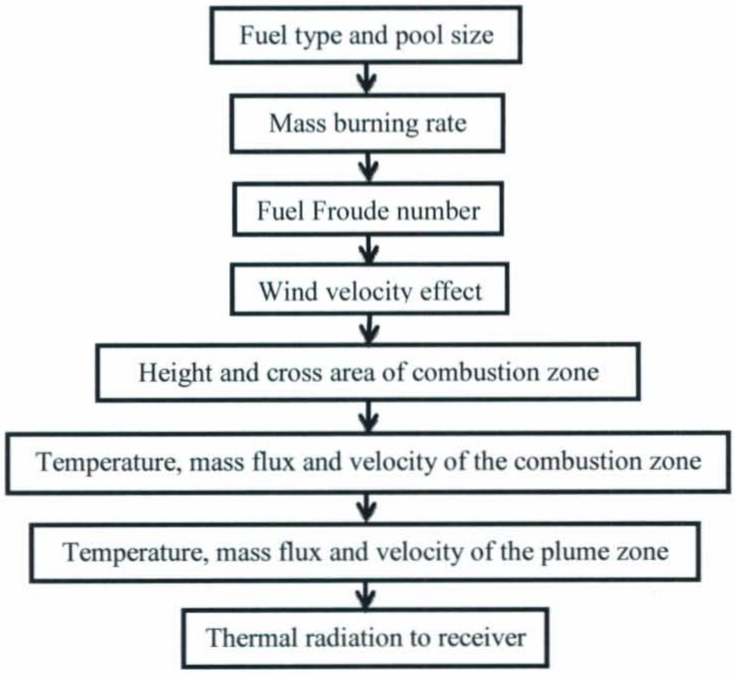

Figure 5.1: Steps which must be followed in the Fay model.

As Figure 5.1 illustrates, the Fay model is a simple, quick and direct approach for pool fire modeling. This model requires fuel properties like heating value and heat of evaporation, stoichiometric ratios, pool size, wind and the environment temperature. Although this model has been verified and calibrated against the results of field tests and has acceptable accuracy, there are some limitations which if overcome, a better and more comprehensive model is achieved.

5.2.2 Proposed Model

In the Fay model, temperature is constant over the height of the combustion zone up to L_c. This does not reflect reality where temperature at the edge of pool base is close to air temperature and in the center of pool base is close to fuel boiling temperature. At the edge of pool base, temperature is controlled by the entrainment flow and at the center temperature is controlled by fuel evaporation. In other words, this model will overpredict the temperature at near ground and subsequently overpredicts the thermal radiation from this section of fire.

Neglecting of heat losses is the main cause of overprediction. Heat losses are important in thermally thin layers like the base of pool fire. To take into account these losses of thermal energy, energy conservation equations Eqs. (3 and 8) are required to be rewritten. To obtain the temperature profile for the combustion zone we have assumed that pool fire is axisymmetric and fuel burning rate per unit volume is the same over the entire combustion zone. This burning rate per unit volume can be obtained as:

$$V = \int_0^{L_c} A_c dz = \int_0^{L_c} \frac{2}{3} {\alpha_c}^{0.5} Dz\, dz = \frac{1}{3} {\alpha_c}^{0.5} D {L_c}^2 \tag{30}$$

$$m' = \frac{\frac{D^2}{4}}{V} = \frac{3}{4} \frac{D}{{\alpha_c}^{0.5} {L_c}^2} \tag{31}$$

Where, m' is fuel burning rate per volume (kg/m^{3}s) and the other parameters are as outlined above. Energy conservation equation is written as:

$$\sum q_c + q_z + q_{z+dz} = 0 \tag{32}$$

Where q_c, q_z, and q_{z+dz} are combustion released energy, inlet/outlet energy at (z) and inlet/outlet energy at (z+dz).

$$q_c = m' V_g h_c; \quad V_g = wA \tag{33}$$

Where, w is the width of the grid and we show later that it will be canceled out from the equation. Vertical heat transfer can be written as

$$q_z = C_p T_z \, w^{\cdot} \, \rho A_c \tag{34}$$

Where $w^{\cdot}$ is average vertical velocity at (z) and T_g is average temperature.

By using Eqs. (30-34), the temperature profile in the combustion zone can be determined. As the temperature in the combustion zone changes, Eqs. (25 and 26) cannot be used to predict thermal radiation. Furthermore, these equations are limited to the combustion zone and the contribution of plume zone in the radiation is not taken into account. In Eqs. (18 to 22) variables such as mass, momentum and temperature are discontinuous in Z = L_c. In addition parameters like temperature and mass flux are incorrectly modeled near the combustion zone. These parameters become accurate when $Z \gg L_c$ and in this situation the temperature is too low and radiation is negligible. To maintain continuity and accuracy of variables in the plume zone, we may rewrite Eqs. (18 and 19) as

$$M_p = M_c(L_c) + \left[\frac{243}{2500}\frac{\eta_p {\rho_a}^2 E_p {\alpha_p}^4}{C_p T_a}\right]^{0.33} (z - L_c)^{1.66}; \ (z \geq L_c) \tag{35}$$

$$P_p = P_c(L_c) + [\frac{5\eta_p E_p}{4\alpha_p C_p T_a \sqrt{\rho_a}}]^{0.4}(M_p - M_c(L_c))^{0.8} \quad (36)$$

The other equations can simply be written as

$$\omega^{\cdot}{}_p = \frac{P_p}{M_p} \quad (37)$$

$$T^{\cdot}{}_p - T_a = \frac{E_p}{M_p C_p} \quad (38)$$

$$A_p = \frac{M_p}{\rho_a \dot{}_p} \quad (39)$$

The variable temperature in combustion zone and rewriting of the plume zone equations imply that we need new equations to calculate thermal radiation to a target. For the radiation of outer boundary, conservation of energy for a segment can be written as

$$q''\Delta A = \int_0^A q''|_{di} dA\,; \quad A = 2\pi di^2 \quad (40)$$

Where, q" is emissive power at a segment of outer boundary with area ΔA, $q''|_{di}$ is the receiving thermal radiation at distance (di) from this segment. Eq. (40) can be rewritten as

$$\sigma T^4 \Delta A = \int_0^A \frac{\vec{n}.\overrightarrow{di}}{di} q''|_{di} dA; \quad (\vec{n}.\overrightarrow{di}) > 0 \quad (41)$$

Where, $\vec{n}$ is the normal of the ΔA and $\overrightarrow{di}$ is the radiation direction vector. Eq. (41) assures that the utmost of thermal radiation is in the direction of ΔA normal. Therefore we can say that for any distance from the ΔA segment $q''|_{di}$ is constant for all the directions and the difference in

receiving thermal radiation is controlled by $\frac{\vec{n}.\vec{di}}{di}$. Therefore $q''|_{di}$ for any distance can be calculated as (see the proof at Appendix A)

$$q''|_{di} = \frac{\sigma T^4 \Delta A}{4di^2} \tag{42}$$

Therefore the thermal radiation which target receives from ΔA segment is

$$q''|_{\Delta A} = \frac{\sigma {T_{\Delta A}}^4 \Delta A}{4di^3}(\vec{n}.\vec{di}) \tag{43}$$

Finally, thermal radiation from the outer boundary can be obtained by integrating Eq. (43) over the entire combustion and plume zones

$$q'' = \sigma \int_0^{A_{ob}} \frac{{T_{\Delta A}}^4(\vec{n}.\vec{di})}{4di^3} dA \tag{44}$$

Where, A_{ob} is the boundary of the pool fire.

Now we can further expand the proposed model to include the effect of surface emissivity on the thermal radiation. Surface emissivity is important, especially in regions like the Arctic where the reflection index of the ground is very high in comparison to temperate or warmer climates due to the presence of snow and ice covered surfaces. These surfaces have higher reflection index and subsequently magnify the thermal radiation which the target receives. For each radiative section according to the target location, there is one specific angle which results in thermal radiation reflection. Therefore we have extended Eq. (44) as

$$q'' = \sigma \int_0^{A_{ob}} \frac{T^4}{4}\left(\frac{\vec{n}.\vec{di}}{di^3} + rf\frac{\vec{n}.\vec{di_r}}{{di_r}^3}\right) dA \tag{45}$$

Where, di_r is the traveling distance vector of reflected beam and (rf) is reflectivity index of the surface.

di_r is always greater then di particularly if the target is close to the pool fire. Another important issue which has not been considered in the previous studies is the absorption coefficient of air which has been taken as zero in above equations. This is valid for most cases since the air absorption coefficient is very low, 5×10^{-6} m^{-1} [45]. However, the presence of water/ice droplets in the air can significantly increase the absorption coefficient of air and subsequently reduce the intensity of radiation. Temperature, wave length, size and the mass per volume of the droplets are the main parameters which affect the absorption coefficient [46, 47]. As the emission from water/ice droplet is much smaller than the energy that they absorb [48], thermal radiation from the droplets has not been taken into calculations.

Absorption coefficient and reflection index of ice and water/ice droplets for a variety of temperatures and wavelengths have been provided in Ref [47, 49-51]. The absorption coefficients of ice and water/ice droplets vary significantly with wavelength. On the other hand and wavelength also determines radiation energy.

$$e_\lambda = \frac{2hc^2}{\lambda^5}\frac{1}{\exp\left(\frac{hc}{\lambda k^{\cdot} T}\right)-1} \approx \frac{2hc^2}{\lambda^5}\exp\left(-\frac{hc}{\lambda k^{\cdot} T}\right) \tag{46}$$

Where, h, c and $k^{\cdot}$ are Planck's constant (6.62×10^{-34} J-S), the speed of light (3×10^{8} m/s) and Boltzmann constant (1.38×10^{-23} J/K) respectively. A differentiation from this equation Eq. (45) determines which wavelengths more contributes into energy transfer.

$$\lambda_{max} = \frac{hc}{5k^{\cdot}}\frac{1}{T}\ ;\ \lambda_{max}(\mu m) = \frac{2897}{T} \tag{47}$$

In the present model, the interval of thermal radiation wavelength, 10^{-8} -10^{-3} m, is divided into N_w wave bands and attenuation is calculated for each band. The widths of these bands are not equal and reduce as wavelength is closer to λ_{max}. For each wavelength band, one needs to calculate absorption coefficient of the air. Assuming that mass per volume of droplets in the air is m_d and droplets have a Gaussian distribution with mean and variance values μ and σ^2 respectively; then, any wave band like the j^{th} with average wavelength λ_j, the corresponded absorption coefficient k_j is

$$k_j = k_{dj}A_d + (1 - A_d)k_a \tag{48}$$

Where, k_{dj}, k_a and A_d are the absorption coefficient of droplet related to j^{th} wave band, pure air absorption coefficient and the relative area of droplets. This relative area is directly related to m_d and is inversely related to droplet diameter respectively. If σ^2 is mathematically equal to 0, then relationship between A_d, m_d and μ becomes (see Appendix B for proof)

$$A_d = \frac{3m_d}{4\rho_d\mu} \tag{49}$$

Where, ρ_d is particle density (kg/m^3). For the cases in which σ^2 is not zero, one needs to integrate this area as

$$A_d = \frac{3m_d}{4\rho_d}\int_{r_d}^{r_u}\frac{cdf(r+dr) - cdf(r)}{r + \frac{dr}{2}}dr; \quad cdf(r) = 0.5\,\{1 + \text{erf}(\frac{r-\mu}{\sqrt{2\sigma^2}})\} \tag{50}$$

Where, (cdf) is cumulative distribution function and r_d and r_u determine the interval of integration. These values are symmetric respect to μ and the size of interval depends on σ^2. For the j^{th} band, the thermal energy after passing a distance (x) in air is given as

$$e_j(x,T) = \frac{2hc^2}{{\lambda_j}^5} \frac{1}{\exp\left(\frac{hc}{\lambda_j k T}\right) - 1} \exp(-k_j x) \tag{51}$$

Where, λ_j is the average wavelength of the j^{th} band. Hence, the total thermal energy which passes through the media (air and droplets) is

$$e(x,T) = \sum_{j=1}^{N_w} E_j(x) = \sum_{j=1}^{N_w} \frac{2hc^2}{{\lambda_j}^5} \frac{1}{\exp\left(\frac{hc}{\lambda_j k T}\right) - 1} \exp(-k_j x) \tag{52}$$

This equation can be replaced into Eq. (45) to obtain the final form of thermal radiation equation

$$q'' = \frac{1}{4} \int_0^{A_{ob}} e(di,T)\left(\frac{\vec{n}.\overrightarrow{di}}{di^3}\right) + rf \times e(di_r,T)\frac{\vec{n}.\overrightarrow{di_r}}{{di_r}^3}) dA \tag{53}$$

Figure 5.2 presents the sequence of steps for the proposed model.

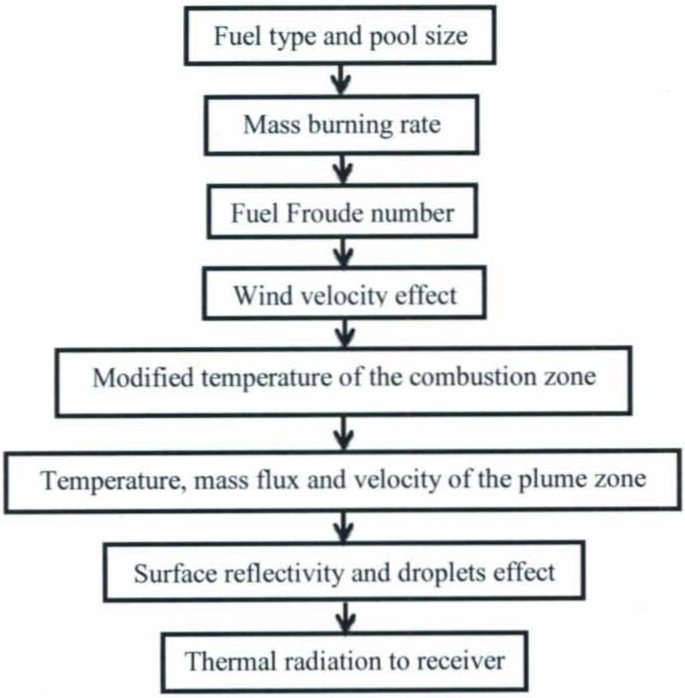

Figure 5.2: Solution steps of the proposed pool fire model.

So far a model has been developed which is capable of including the environmental parameters effects on the behavior of pool fires. The main environmental parameters for the Arctic region are snow/ice covered surfaces and droplets. In the next section we will see how these two parameters can affect the thermal radiation intensity from a pool fire. The quantitative comparison between the proposed method and the Fay model is explained through a pool fire modeling case study. Here, we use a pool fire of gasoline with 1.4 m diameter to illustrate these models. The assumption is that there is no wind.

5.3 Results and Discussions

5.3.1 Proposed Model versus Fay Model

The Fay model was revised and extended to include the effect of environmental parameters like surface reflectivity and the presence of water/ice particles. As mentioned by Fay [33], his model is discontinuous at $Z = L_c$. An example of this discontinuity has been shown in Figure 5.3 for the purpose of illustration. The main reason of this discontinuity is that vertical energy transport due to mass movement has not been considered in the combustion zone and subsequently this zone has a constant temperature. The initial temperature of the plume zone depends on the coefficients, particularly η_p. Figure 5.3 shows temperature in the plume zone for three different η_p. The major issue of using Fay model is that there is no a specific value or method to obtain η_p and as Figure 5.3 shows that temperature highly depends on this parameter.

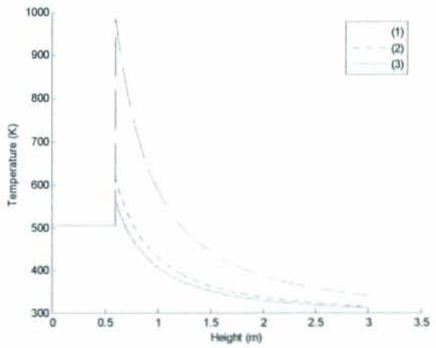

Figure 5.3: Temperature distribution for Fay model; very small η_p (1), small η_p (2) and medium η_p (3). Temperature is discontinuous in the intersection of zones.

To avoid these issues, discontinuity in the temperature and not having the exact value of η_p, the temperature profile in the combustion zone has been modified (Figure 5.4). The new

distribution of temperature is the result of considering heat transfer between different heights in the combustion zone. As temperature is continues, the initial temperature of the plume zone is set equal to the temperature at the end of combustion zone.

In Figure 5.4 the integral of temperature curves for both models, the Fay model and the present model, are the same and the total released energy is the same for both cases. However in the present model, the temperature is low near the pool surface and it increases with height as the released energy rate increases and energy is transferred upward due to hot gases movement. Furthermore, the radiation equation which has been used in the Fay model uses an average temperature and ultimately underpredicts the radiation flux. Thermal radiation fluxes for both models have been compared in Figure 5.5. The difference is higher near the pool fire and as the radial distance increases this difference reduces.

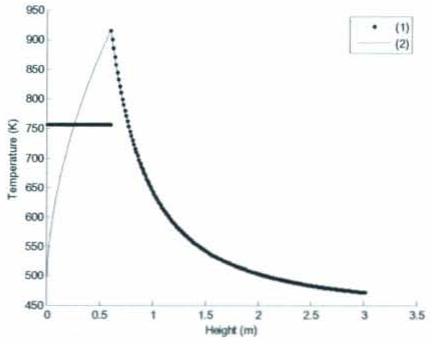

Figure 5.4: Temperature distribution for different models, Fay model (1) and new model (2).

Thermal radiation fluxes for both models have been compared in Figure 5.5. The difference is higher near the pool fire and as the radial distance increases this difference reduces.

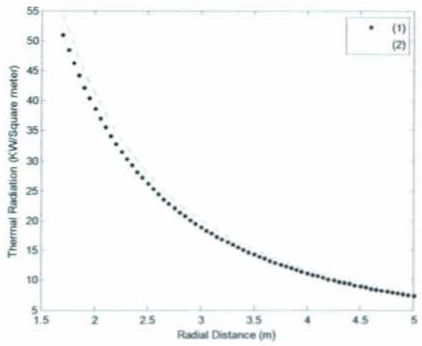

Figure 5.5: Comparison of predicted thermal radiations; Fay model (1) and the proposed model (2) at height 1.0 meter.

Another major limitation in the Fay model is not considering radiation from the plume zone as it cannot account for radiation where the temperature profile is not constant. Neglecting the plume zone might be reasonable when the height of combustion zone is large or when the target is near ground. However, for the cases where the target is high, radiation from the plume zone cannot be neglected. The thermal radiation flux of plume zone which has been calculated by the proposed model is shown in Figure 5.6. This figure clearly illustrates the plume zone contributes more at higher heights; although, the total radiation from this zone might be small compared to the combustion zone. Figure 5.7 demonstrates the percentage of plume zone contribution compared to total radiation flux which a target receives. This figure shows that plume zone contribution for higher heights is more important compared to lower heights. Therefore, neglecting radiation from the plume zone results into severe underestimating of radiation flux in the high heights.

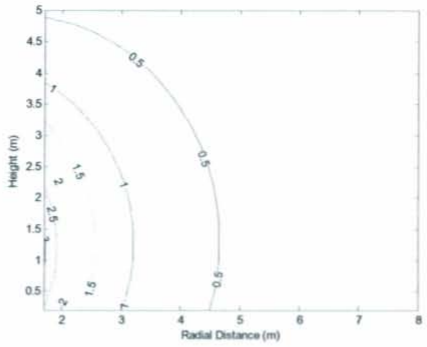

Figure 5.6: Contribution of plume zone in thermal radiation flux (Kw/m^2).

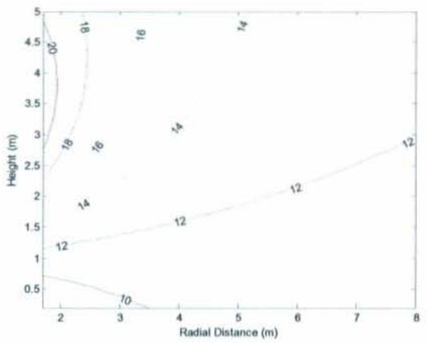

Figure 5.7: Percentage of plume zone contribution in the total radiation flux.

Figure 5.7 also illustrates that as the radial distance increases, the influence of plume zone decreases and combustion zone dominates the thermal radiation flux. At large radial distances, even for high heights, the radiation from the plume zone becomes negligible compared to combustion zone. In this case, the radiation angle and the distance to the target becomes almost same for both plume and combustion zones.

5.3.2 Surface Reflectivity

Although the plume zone share in the thermal radiation is small compared to the combustion zone, neglecting it results into underestimating of thermal hazards. Therefore, the plume zone radiation has been considered in all subsequent sections. After correcting temperature distribution and including the plume zone in thermal radiation, we may investigate the effect of surface reflectivity on the thermal radiation. The Fay model does not account for this parameter or we can say that the surface reflectivity is 0 for this model. In snow and ice covered surface, the surface reflectivity may be as high as 0.93.

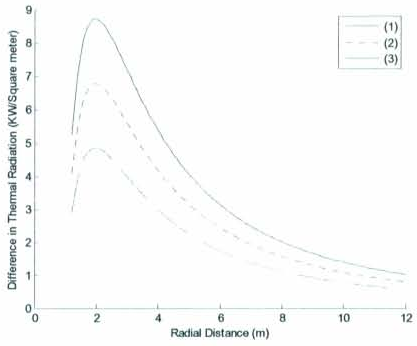

Figure 5.8: Difference (proposed model – Fay model) in the receiving thermal radiation at height 1.0 m; surface with reflectivity index 0.9 (1), reflectivity index 0.7 (2), reflectivity index 0.5 (3).

In Figure 5.8, the difference in thermal radiation flux predicted by the Fay model and the proposed model is shown and illustrates as surface reflectivity increases, the Fay model underestimates radiation. Furthermore, surface reflectivity has small contribution to the thermal

radiation for very close distances or far away from the pool fire. The reason of this small contribution is that at short distances the reflection has a very large angle and the second part of Eq. (45) becomes negligible. Finally the difference reduces as radial distance increases.

We expected that the contribution of reflection reduce as height increases. The reason of this behavior is that both reflection angle and distance increases with height. However, this is not always the case and near the surface at approximate height of 0.4 to 0.7 m, as shown in Figure 5.9, the reflection contribution increases slightly. This behavior is due to the radiation from the top of combustion zone, from the bottom of plume zone and the reflected thermal radiation. Except the slight growth in the reflected thermal radiation, reflection contribution reduces as height increases. A comparison between Figure 5.10.a and Figure 5.10.b shows that the thermal radiation distribution changes significantly with reflection.

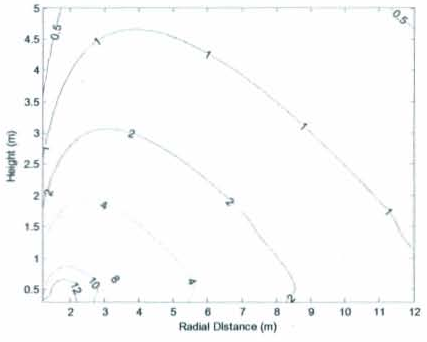

Figure 5.9: Reflection contribution in the thermal radiation.

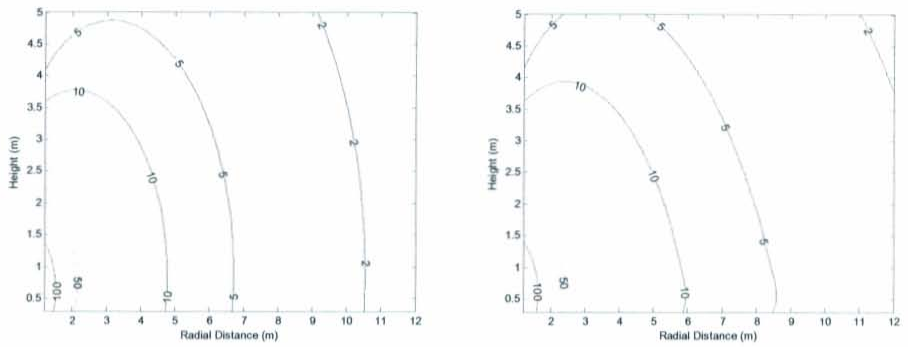

Figure 5.10: Thermal radiation flux; a: surface reflectivity index is 0.0 and b: surface reflectivity is 0.9.

5.3.3 Droplets Effects

The proposed model was further extended to include the effect of water/ice droplets. The introduction of droplets into the air reduces transparency of air, increases the extinction coefficient of the air and subsequently results into higher attenuation of thermal radiation flux. The attenuation depends on parameters such as pool fire temperature, wavelength and droplet kind, size, distribution and mass concentration in the air. Here the effect of droplet size, distribution, mass concentration and droplet kind (water or ice) has been examined.

Figure 5.11 presents the thermal radiation flux for several cases. In this figure, variance is considered zero (all droplets have the same size in each case). The mass concentration for cases 2-4 is the same. As shown in Figure 5.11, large droplets have negligible effect on the thermal radiation (comparing cases 1 and 2). However, as droplet size reduces the attenuation increases and for small droplets the attenuation of radiation is rapid (case 4).

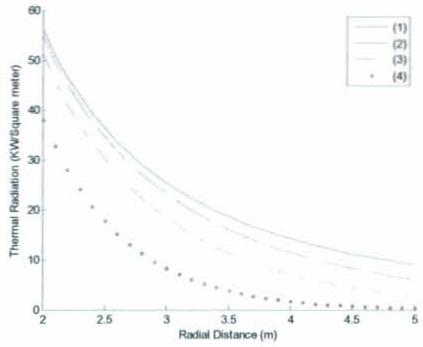

Figure 5.11: Attenuation of thermal radiation flux for different droplets sizes; no droplet in the air (1), very large droplets (D = 400μ) (2), large droplets (D = 100 μ) (3) and medium droplets (D = 20 μ) (4).

Figure 5.12 demonstrates the effect of droplets size distribution on thermal radiation. As the variance increases, thermal radiation reduces more due to the presence of smaller particles in the air. It must be noted that as the mean size of droplets reduces, variance becomes more important.

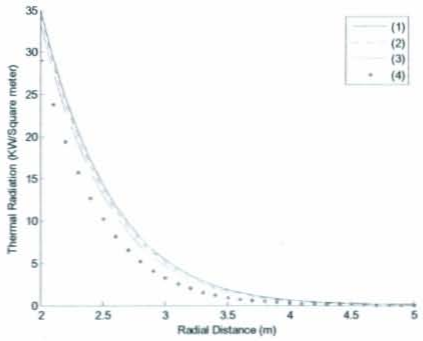

Figure 5.12: The effect of droplet diameter distribution on thermal radiation extinction; for all cases the mean diameter is 5μ and distribution is Gaussian; $\sigma^2 = 0.0$ (1) (all droplets have the same diameter), $\sigma^2 = 1.0$ (2), $\sigma^2 = 2.0$ (3) and $\sigma^2 = 5.0$ (4).

The relationship between attenuation coefficient and the mean size of droplets is observed to be an inverse relationship. Eq. (50) indicates a direct relation between mass concentration and attenuation coefficient. Figure 5.13 shows that as mass concentration increases, thermal radiation decreases.

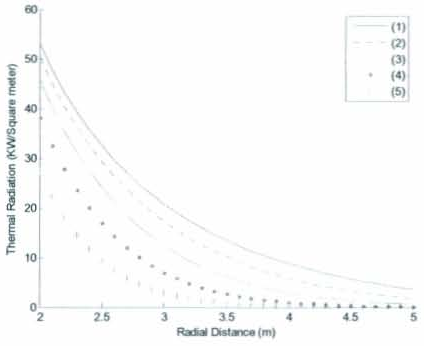

Figure 5.13: Effect of droplet mass concentration on the attenuation of thermal radiation; $m_d = 5$ gr/m^3 (1), $m_d = 10$ gr/m^3 (2), $m_d = 20$ gr/m^3 (3), $m_d = 40$ gr/m^3 (4) and $m_d = 80$ gr/m^3 (5).

Figure 5.14 shows the impact of water droplet on the thermal radiation. Case 1 refers to the presence of water droplets in the air while in Case 2 there is no water droplet. At each height, the difference increases gradually with the radial distance until reaching a peak and then decreasing. Over long distances the difference reduces since the thermal radiation of both cases decreases significantly.

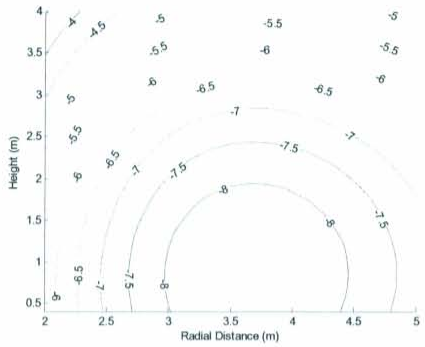

Figure 5.14: Difference in receiving thermal radiation (Case 1 – Case 2), $m_d = 10$ gr/m^3, D = 50 μ. For this case the surface reflexivity has not been considered.

5.3.4 Arctic Region Conditions

Figure 5.8 to Figure 5.14 indicate that surface reflectivity and the presence of water droplets have significant and opposite effects on the thermal radiation flux. While surface reflectivity amplifies thermal radiation, the presence of water droplets results into a faster attenuation of radiation. Therefore, it is expected that the interaction between these two parameters result into a more complicated pattern. Figure 5.15 demonstrates an example of this interaction. This figure shows the difference between Cases 1 and 2. Case 1 refers to arctic condition where a high surface reflectivity and water droplets coexist. In contrast, Case 2 is for a scenario where surface reflectivity is low (0.1) and there is no droplet in the air.

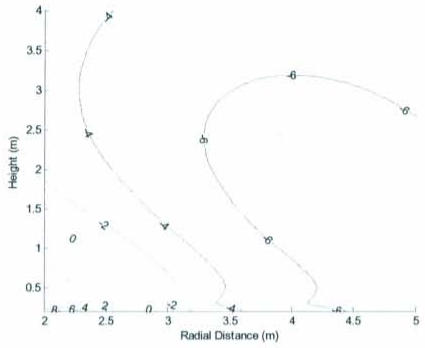

Figure 5.15: Difference in receiving thermal radiation for arctic conditions (Case 1– Case 2), m_d = 10 gr/m^3, D = 50 μ and ref = 0.9 for Case 1.

As shown in Figure 5.15, the thermal radiation flux is higher in Case 1 for short distances and low heights. The distance and the height at which thermal radiation of Case 1 is higher depend on the pool fire diameter and fuel type. For short distances and low heights, reflection compensates for the effect of water droplets because of small reflection angle. For larger heights, the reflection angle is large and subsequently water droplet becomes the dominant parameter. It is to be mentioned that these result also depends on the wavelengths which depends on the pool fire temperature. Hence, for a different temperature distribution of the pool fire, the results might be significantly different as the absorption coefficient of water droplets highly depends on the wavelength.

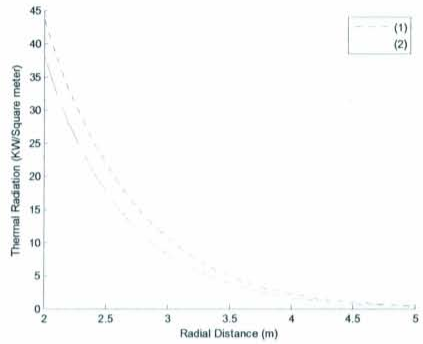

Figure 5.16: Effect of different type of droplets on the thermal radiation extinction, water droplets (1) and ice droplets (2).

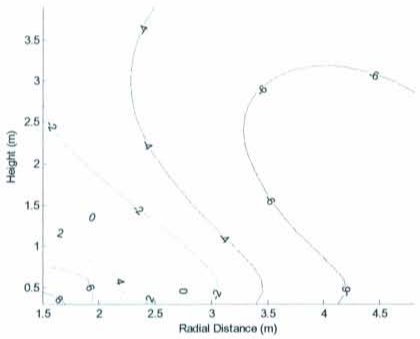

Figure 5.17: Difference in receiving thermal radiation at the presence of ice droplets (Case 1– Case 2), $m_d = 10$ gr/m^3, D = 50 μ and ref = 0.9 for Case 1.

The effect of ice droplets versus water droplets has also been modeled and compared in Figure 5.16. The mean value, variance and mass concentration are the same for both ice and water droplets in this figure. For the specified pool fire with its specific temperature distribution, ice droplets result in less thermal radiation reduction compared to water droplets. As such, surface reflectivity becomes the dominant affecting parameter up to a larger radial distance and height as shown in Figure 5.17. In this figure, all the parameters are the same as Figure 5.15

except the absorption coefficient which is the absorption coefficient of ice. In general we can say that for the Arctic compared to a more temperate region, the thermal radiation is higher for short distances and is lower for large distances.

Chapter 6: Explosion Modeling

This chapter provides required information about explosion hazard and its consequence assessment. Explosion is the second most frequent accident in both offshore and onshore facilities. In explosion modeling, generated overpressure is the most important parameter which determines the level of accident and its consequences. Many different types of explosions may occur . These explosions categorized as unconfined (overpressure is mostly related to the presence of obstacles), confined (overpressure is related to confinement and obstacles level), physical explosion (failing of pressurized vessel) and solid explosion. For oil and gas industries, gas explosions are the major hazard.

This chapter divides explosion modeling into three main categories: Empirical models, Phenomenological models and CFDs. Empirical models are the easiest and quickest models to predict overpressure. These models estimate generated overpressure based on correlations which have been obtained from large scale experiments. These correlations simply relate generated overpressure into parameters like distance and released energy. Therefore, there is no or less explosion physic in these models. In contrast, phenomenological models represent the physics of explosion in its simplest way. On the other hand, CFD models describe and employ a detailed physics through solving explosion governing equations. Therefore, these CFD models provide the most accurate and detailed result for explosion phenomenon.

6.1 Explosion

Explosion is defined as a sudden release of energy associated with an increase in pressure and temperature [52]. Gas explosion are generally defined as either confined or unconfined. For example explosion inside a vessel or building is a confined explosion. For fully confined

explosions (no ventilation, opening and heat loss) there generated overpressure could be up to eight times of initial pressure. However, generated overpressure is mainly determined by the temperature ratio of burned gas to unburned gas.

Explosion in low congested confined places has low initial turbulence and therefore low flame speed. In the presence of obstacles, flow would be more turbulent and result in higher combustion rate and flame acceleration and hence higher flame speed. If flame and combustion zone propagate in a speed higher than sound velocity in comparison to unburned front gases, detonation occurs. Detonation is a self-driven shockwave where reaction zone and overpressure pulse are coupled and propagate together. In this case, the reaction initiates by compression heating of shockwave. Although the possibility of occurrence for this kind of overpressure is relatively low, it is the most hazardous accident. Detonation overpressure and its propagation speed could reach up to 20 bars and 5 Mach respectively. If the relative speed of reaction zone to unburned gas is less then sound velocity, then deflagration occurs. In this case reaction zone propagate due to molecular and/or turbulent diffusion.

In explosion modeling turbulence is the main factor which controls flame speed, shock speed and generated overpressure. Turbulence is produced and controlled by obstacles; thus, generated overpressure is very low when there are no obstacles or obstacle density is low. As flow passes through obstacles, turbulence grows and results in more flame area and therefore higher combustion rate due to higher diffusion and convection. Growth of combustion rate increases the explosion flow and hence the turbulence is magnified again. This cycle provides high combustion rate and generated overpressure.

6.2 Effective Parameters in Explosions

The consequence of an explosion depends on generated overpressure, during of shockwave interaction with objects, duration of negative pulse after shockwave and etc. These characters of explosions depend on several parameters: blockage ratio, confinement and ventilation, congestion and geometry, fuel type, ignition source and location, ignition time and fuel-air mixture stoichiometry and initial turbulence level [52].

Blockage ratio is criterion which determines how and up to what level a structure is congested. Typically larger blockage ratio results in higher generated overpressure. However, size, shape and location of objects also have a significant effect on the outcome of an explosion. For instance, for similar size and blockage ratio smaller obstacles provides more overpressure. Generally as the flame passway becomes narrower and more tortuous, overpressure is expected to be higher. This is mainly due to flame area expansion and higher turbulent flow.

Fuel type plays a critical role in explosion phenomenon. As the reactivity of fuel increased, generated overpressure would be higher. For example, hydrogen explosion generates a much higher overpressure than Methane and ethane. Ignition source also has a significant rule. For example, source point ignition point results in lower overpressure in comparison to jet-type explosion.

6.3 Modeling

There are three different approaches for modeling an explosion scenario: using empirical correlations, phenomenological models and CFD models. Among these three categories, empirical correlations are the simplest which do not care of the explosion physic; therefore, they are easy and quick models. In contrast CFD modeling is the most complicated and detailed

approach which requires larger preparation and computational time. Phenomenological models are somewhere between CFDs and empirical correlations.

6.3.1 Empirical Models

These models have mostly been developed base on experimental data. They share characteristics like being fast, calculation overpressure for a distance from the center of explosion and etc. They simply relate the generated overpressure to parameters like scaled distance, released energy, flame speed, fuel reactivity and etc. widely used empirical models have been described briefly in below.

6.3.1.1 TNT Method

The main assumption of this method is that gas explosion is somehow similar to high charge and solid explosives like TNT. The TNT equivalency model employs scaled distance-scaled pressure curve to estimate pick of overpressure. In this method, TNT mass equivalent to the hydrocarbon mass in vapor cloud is calculated. Moreover, an experimental factor is used to compensate for differences in the physic of explosion. This experimental factor was initially set to be 0.3-0.5 and as the model was later modified, 0.2 was assigned for the factor. Furthermore, the model was modified to take into account the geometry.

The main weakness of this model is that gas explosion nature is extremely different from solid explosion. For example, detonation of TNT shockwave is much more rapid than vapor cloud explosion. As a result TNT near filed overpressure is much higher in comparison to generated overpressure of gas explosion. Subsequently, in close distances from explosion center, this model predicts very high values for overpressure pick [52, 53]. Moreover, determining

explosion center is difficult since in most of cases hydrocarbon mass center is not the explosion center. Furthermore, this model just provides information for positive phase.

6.3.1.2 Multi-Energy Method

Multi-energy method has been used widely to estimate explosions overpressure. The model was developed based on the numerical simulation of centrally ignition of a spherical vapor cloud [52-55]. This model calculates overpressure based on the portion of gas which has been confined or blocked by obstacles. The behind concept for such a consideration is that part of cloud which is unconfined will generate a slight overpressure if ignited.

This method requires two parameters: energy scaled distance and explosion strength. This energy scaled distance somehow determines how much of released energy contributes into overpressure generation in a desired distance. Explosion strength is a number from 0 to 10 where 10 represent detonation and 0-9 are used for deflagration. After finding energy scaled distance and explosion strength, a set of curves are used to determine scaled overpressure and positive phase duration.

The main advantage of this method over TNT is that explosion strength has been considered as a variable parameter which could differ from a scenario to another one. Moreover, the results are more realistic especially for near field where TNT overestimates extremely. However, determining explosion strength is a difficult issue. Furthermore, it fails to accurately represent a complex geometry. There is not a unique and clear way to deal with several congested areas, multiple blast waves or multiple ignition sources.

6.3.1.3 Baker-Strehlow Model

Baker-Strehlow (BS) model is similar to multi-energy model. In both methods, presence of obstacles results into higher intensity explosions. While in multi-energy model explosion strength is dominant parameter, flame speed is the main parameter which determines overpressure in BS model. Energy scaled distance is similar for both of these models. Flame propagation speed is determined through BS matrix [56-59]. There are three qualitative factors which specify the flame speed of a scenario: the ways or domains in which flame front could propagate (1D, 2D or 3D), fuel reactivity and density of obstacles. Then, scaled overpressure is calculated from correlations or read from curves.

This model is easy to use and also consider some geometrical aspects of structure specially congestion. Moreover, it could handle multi-ignition explosions. Since this method has been developed based on experimental data, it is expected to be more reliable and realistic in comparison to multi-energy method. Nevertheless, this model is overconservative and moreover, obstacle density is a subjective issue.

6.3.1.4 Congestion Assessment Method (CAM)

The Congestion Assessment Method (CAM) takes into account plant layout (congestion and confinement) and fuel type to predict overpressure of explosions [52]. This model has been developed by Shell Thornton Research Centre based on wide variety of experimental results. The accuracy of this model is fairly acceptable, although it has been developed to obtain conservative results. The first step in this method is to determine a reference pressure P_{ref} is congested area. This P_{ref} is an estimation of pick overpressure which an explosion could generate. After that fuel is taken into account through a fuel factor which is multiplied into P_{ref} to determine source

pressure for selected type of fuel. Finally, overpressure for various distances is estimated by a pressure decay curve.

This model has been further modified and improved based on large scale to small scale experiments to address problems like non-symmetric plants, plants which are much longer in one direction in comparison to the other two directions, when gas volume is smaller than congested volume (partial filling) and how to deal with sharp edge objects. Because of these modifications, this model is the best empirical model especially when it is applied for layouts on which model has been calibrated.

The most challenging part is determination of congestion level. Although, there are guidelines for congestion and confinement assessment, this yet a subjective engineering practice. If two individuals attempt to determine congestion level and generated overpressure, while they may get similar results for simple plants; for complex plants the results could be significantly different.

This model predicts better than other empirical models since has been calibrated over numerous different scale experiment. Furthermore, it is easy to use and permits for non-symmetric or long narrow plants. However, like other empirical models, it cannot take the details of plants. Table 9.1 represents the list of empirical models and a brief description.

6.3.1.5 COMEX

COMEX, COMpiled EXplosion model has been developed for overpressure calculation in partially confined areas. The model is only applicable for propane [60]. Five different models have been implemented in the code: two of them for overpressure prediction in confined spaces and the other three for spaces with venting. The code is an Excel spreadsheet and will run on PCs

if an Excel or an Excel compatible spreadsheet has been installed. This model is applicable for low two dimensional spaces; where the ratio of height to other two dimensions is low.

Array of obstacle with blockage ratio could be defined in this model. Moreover, model takes into account the shape and direction of obstacles. However, all defined obstacles must have identical size and shape. Furthermore, this model is limited to vapor cloud explosion of propane. Table 6.1 presents the summary of empirical models.

Table 6.1: List of selected empirical models with brief descriptions.

Model	Description
TNT	Assumes that gas explosion is somehow similar to solid explosion, highly overestimates for near fields and does not take into account geometry.
TNO	It is similar to multi-energy method, assumes that all gas vapor contributes into explosion.
Multi-Energy Method	Assumes that the congested and confined part of cloud contributes into explosion, provides information about the duration of positive phase.
Baker-Strehlow	Calculates overpressure based on flame speed, takes into account the flame pass way and fuel reactivity, results are conservative.
Congestion Assessment Method	Calibrated over numerous experiment results, allows for calculation of non-symmetric or narrow plants, it could deal with sharp edge objects and partially filled congested area.
Sedgwick Loss Assessment Method	Has been developed based on CAM idea, some modification has been done.
COMEX	uses 5 different correlation for prediction overpressure prediction, can handle shape and direction of obstacles

6.3.2 Phenomenological Models

The physics of explosion could be described either empirically or theoretically. While empirical models attempt to represent the physic of explosion by correlation and curves which have been developed based on experiments; CFD models employ mathematically governing equations to illustrate the physics [52]. Phenomenological models are somewhere between CFD

models and empirical models. On the other word, they employ the physic as simple as possible and only include essential physics. The major simplification is in geometry representation. Indeed, the actually geometry of scenario is not modeled and a simplified and idealized geometry is used. This idealization provides accurate approximations for simple cases; however, for more complex geometries phenomenological models fail to provide accurate outcomes.

Since phenomenological models implement simple physics and geometry, they are fast in calculation and run-time is usually in the order of second. This characteristic makes them suitable for optimization practice. A large number of preliminary designs and situations could be modeled quickly to achieve a limited number of preliminary acceptable situations. Then a detailed analysis could be done either by performing experiment or CFD modeling.

6.3.2.1 SCOPE

The SCOPE (Shell Code for Overpressure Prediction in gas Explosions) model has been developed in Shell Thornton Research Centre [52]. This model has initially been developed for gas explosion modeling in offshore structures. This is a one dimensional model which simply takes geometry as a vented vessel with some obstacle grids. The obstacle grids determine the turbulence and turbulent combustion. Since SCOPE is one dimensional, it may be used wherever, flame passway is single and/or one dimensional.

This model takes into account the length and volume of compartment. Moreover, size, location and shape of vent have been considered in calculations. Standard compressible vent flow equations have been used to consider flow from vents. Also the effect of external explosion from vented unburned gas has been taken into account. For vented gas, the assumption is that it forms a mushroom shape vapor cloud.

This model predicts overpressure for the worst case by putting the ignition point in the opposite face of compartment where distance between ignition point and vent is maximum. Flame is assumed to be semi-spherical until it reaches the walls of compartment. In order to correctly estimate the generated overpressure and vented gas, flame position, unburned and burned gas masses are calculated by two simplified differential equations along with several other equations for turbulent velocity and etc.

SCOPE has been validated and calibrated against large number of experiments with different size, congestion and fuel type. Moreover, it could simply handle geometry and ventilation. These properties make SCOPE a suitable model for initial phases of structure design. However, these idealizations cease deviation for modeling a complex scenario. Moreover, it only models a single enclosure and possible external explosion related to the enclosure. Therefore, it could not be used for the cases in which ignition happens outside the compartment.

6.3.2.2 CLICHÉ

The CLICHÉ (Confined LInked CHamber Explosion) has been developed by Advantica Technologies Ltd to simulate gas explosion in confined structures. The idea is based on the vented vessels which are connected. The reason is that plants could be considered as semi-confined and congested areas which are connected together. Therefore, CLICHÉ is a generalization of interconnected confined areas.

CLICHÉ solves a set of ordinary differential equations which describe chambers. Conservation low for unburned and burned gas is applied in each chamber. Inside each chamber, the assumption is that properties are uniform and momentum changes only in the boundaries of connection links. This assumption does not permit flow distribution and flame distortion in

chambers. Therefore, flame distortion is determined by applying empirical correlation based on chamber volume and burned gas.

Since this model utilizes a numerically generated flame area, ignition point could be set for any desired location. Moreover, rate of flame growth is calculated based on unburned gas velocity. As flame intersects an obstacle, it becomes turbulent. Turbulence parameters are determined based on flow velocity and obstacles. CLICHÉ can also handle external explosions.

6.3.2.3 NVBANG

NVBANG is used to calculate the generated overpressure as a function of time for partially confined volume [60]. This model has no sub-model for overpressure generation; thus, it is used along with other models which could provide overpressure. The procedure is to adjust the NVBANG parameters so that NVBANG generate same overpressure. If COMEX has been used along with NVBANG, a set of parameter could be changed so that NVBANG be applicable for other fuels.

Ventilation could be obtained by pressure relief panels. The pressure relief panels could be specified on any wall and there is no restriction on the area else vent area exceeds the wall area. NVBANG could not handle obstacles or external explosions directly; therefore, feedback factor is calibrated after inputting data from another model. Moreover, feedback factor is used for calibration of burning velocity in turbulent flows. Burning velocity in turbulent flows has been defined as laminar burning velocity times the feedback factor. Therefore, presence of obstacles calibrates and increases feedback factor and this feedback factor is used to correct burning velocity.

This model assumes that the shape of flame is spherical until it reaches the boundaries where it transitions to a semi spherical zone. The other assumption is that the released energy is distributed uniformly in the volume of burnt gas and the burnt gas expands adiabatically.

This model is easy to use, and the computational time is comparatively low. Moreover, venting and connected modules could be simulated with this model. The main drawback of this model is that it requires another model for overpressure generation. In addition, there is no clear method to deal with input parameters, particularly the feedback factor which controls the burning velocity. The model also assumes that the energy is distributed uniformly in volume of burnt gas and the burnt gas has an adiabatic expansion. This results in a unrealistic uniform overpressure for the entire domain.

6.3.3 CFD Models

Computational Fluid Dynamic (CFD) models approximate the solution of a set of partial differential. Navier-Stokes equations which describe flow and sub-models (e.g. combustion and turbulence) are solved simultaneously [52, 61 and 62]. Domains (both time and space) are discretized and coupled algebraic equations are solved iteratively.

CFD models predict temperature, pressure, velocity, density and species concentration in detail. This is the main advantage of CFD models over two previous models. In addition, CFD modeling can provide precise information where conducting experiment is impossible or impractical. The other main advantage of CFD models is that they are sensitive to details and therefore allow slight design or scenario modification and simulation. The main limitation of CFD models is their computational time. For example, it is impractical to simulate a small scaled

turbulence in explosion process. Therefore, turbulent sub-models have been developed to simplify the turbulence phenomenon and reduce computational time.

6.3.3.1 AutoReaGas

AutoReaGas has been developed by TNO and Century Dynamic Ltd. This model utilizes ReaGas sub-models for gas explosion solving and BLAST for shockwave propagation. ReaGas is a three dimensional finite volume code which employs Cartesian grid. First order schemes have been used for both time and space discretizing. The Turbulence modeling is performed by classical k-ε model and the SIMPLE algorithm is used for pressure correction. While large obstacles are usually resolved by grids, small obstacles are taken into account through a porosity distributed resistance. Small obstacles are considered as extra source of turbulence in the system.

The combustion is assumed to occur as a single step reaction where the reaction rate is obtained from empirical correlations for different flame speeds. The transition from laminar to turbulent combustion is controlled by local flow conditions. To account for the reality that the gas-air mixture is not uniform, a mixture fraction has been introduced. Therefore, equations are approximated for mixture fraction and fuel mass fraction.

One of the most important strength of this model is that it has been calibrated over small to large scale experiments. Furthermore, BLAST can be used to study far field effects and a large number of objects can be introduced in the model. Also a water deluge sub-model is included. However, this model uses first order schemes for solution approximation.

6.3.3.2 CFX

CFX is a general purpose finite volume code which used for explosion modeling of complex geometries as the model generates multi-block and non-orthogonal grids. A variety of solvers and sub-models are available among which user can select the appropriate one. For example, first order or second order schemes could be selected; k-ε or Reynolds stress turbulence model may be chosen for turbulence modeling.

Temporal differentiating schemes are either first order accurate (backward Euler or implicit Euler) or second order accurate (Crank-Nicolson). The Euler scheme is positive definite and can be used with relatively large time intervals. The term "positive definite" is referred to a scheme which converges without any restriction on the stepsizes. In contrast, Crank-Nicolson scheme is not bounded for positive definite variable; therefore, small time steps are required. CFX also provides higher order temporal differentiation by employing backward differentiation methods. These schemes are used to improve the drawbacks of previously mentioned schemes.

The main advantage of using CFX is the flexibility offered from the variety of discretizing schemes. The multi-block meshing offers a much better control over mesh generation. The model has also been tested and calibrated against experiments especially for methane and hydrogen explosion modeling. However, for other gases, the model shows poor agreement with experimental results [52].

6.3.3.3 COBRA

COBRA is a finite volume code which employs adaptive mesh generation algorithm. This model applies an unstructured meshing which could be refined and de-refined automatically to insure efficiency and accuracy of solution. The grid is updated after each time step to maintain

an acceptable resolution of flow characteristics. Employed mash structure could be either Cartesian or cylindrical. Although grids are refined in each time step, COBRA uses Porosity Distributed Resistance (PDR) for obstacles which have not been resolved by grid. The integration scheme is second order both temporally and spatially. Therefore, all flow properties are approximated in the center of computational cells. However, for some studies, the model outputs have significant difference with experiments. Moreover, it employs two-layer-k-ε turbulence model. The main disadvantage of this turbulence model is that it uses algebraic equations for near-wall domains. Finally, there is no sub-model to account for flow transition from laminar into turbulent.

6.3.3.4 EXSIM

EXSIM is a finite volume code which has been developed by Shell Global Solution and Telemark Technological Centre. Structured Cartesian gridding is employed with PDR to capture the effects of small obstacles which may have not been resolved by grid. Like models which have been presented previously, EXSIM uses the k-ε model for turbulence modeling. The time discretizing scheme; the space discretizing scheme could be either first order or second order accurate.

The results of computations have been compared with numerous experiments. The model is appropriate for a variety of congestion and confinement scenarios up to a completely unconfined geometry. The major weakness of model is using low order accurate schemes (mainly first order schemes) and mesh refinement/ de-refinement has not been considered for this model.

6.3.3.5 FLACS

FLACS (FLame ACceleration Simulator) is also a structured Cartesian grid, finite volume, k-ε turbulence based model like EXSIM. The general discretizing scheme is a first order central scheme and a second order scheme has been used for reaction progress. The combustion model used is a β flame model that uses correlations of turbulent burning velocities. The β model assumes flame thickness and burning velocities as constant and the flame curvature is adjusted by correction functions.

FLACS has been compared and calibrated versus a number of small to large scale experiments and results are reported to be in good agreement with experiments (± 30% error in overpressure approximation). FLACS contains a water deluge model. The main drawback of FLACS is the absence of an adaptive gridding algorithm. Thus, the user needs to modify mesh sizes after the run is completed and run again. Furthermore, the scheme is first order and therefore, smaller computational cells are required to obtain reasonable result. This may increase computational time dramatically.

6.3.3.6 NEWT

NEWT is finite volume code with adaptive unstructured mesh which makes it suitable for modeling of complex geometries. A fourth order Runge-Kutta integration method is used for temporal integration. This high order scheme allows for choosing larger time steps and subsequently less computational time is required. A combination of second and fourth order is used for spatial discretizing. For turbulence modeling, a modified k-ε model is used.

The combustion sub-model is an eddy break up or laminar Flamelet model. The eddy break up model may result into wrong predictions for gases ignition ahead of the flame. This is

corrected by suppression of the leading edge of the flame at the end of each time step. In contrast, the laminar Flamelet model does not need corrections and shows better agreement with experimental data. However, using laminar Flamelet model increases the computational time.

This model incorporates an adaptive and automatic mesh algorithm which could be used easily for complex geometries. However, model outcomes are not in good agreement with experiments results. These deviations are mostly related to implement of inaccurate ignition model, inaccurate modeling of the initial development of laminar flow, inaccurate transition from laminar into turbulent flow and finally using simple k-ε model.

6.3.3.7 REACFLOW

REACFLOW is a finite volume code which has been developed for gas flow with chemical reaction simulations. Like NEWT, it utilizes an unstructured mesh algorithm which is suitable for complex geometries. The discretizing scheme is either first or second order accurate spatially and first order accurate temporally. In REAFLOW, there are two different sub-models for combustion modeling: finite rate chemistry and eddy break-up model. Finite rate chemistry is used when the turbulence effects are negligible e.g. laminar flame. For turbulent combustion, eddy break-up model is used. The main drawback of this model is related to implementation of these simple combustion models. Moreover, the integration schemes are low order accurate, therefore, smaller temporal step sizes and spatial computational times are required.

Chapter 7: Explosion Consequence Modeling in Arctic Region

Previous chapter covered different methods and models for explosion consequence assessment. However in the arctic regions, the presence of snow and ice covered surfaces adds complexity to the explosion phenomenon. Snow may compact, displace and absorb considerable portion of explosion energy and impacts the generated overpressure, shock wave profile and its propagation, calculated risk and finally decision making. Although there are numerous CFD (Computational Fluid Dynamics) models which could be used for explosion modeling, most of them could not take into account the presence of snow and approximate its behavior. Moreover, coupling governing equations of explosion and governing equations of snow is computationally challenging. These challenges raise both in implementation and computation costs. There are empirical models which could be used; however, none of them have been tested and calibrated for explosion over snow. This chapter makes an attempt to integrate an empirical explosion model with snow model. Baker-Strehlow is used as the explosion model along with snow model, called jump equations, to modify and adopt Baker-Strehlow over snow covered surfaces. Risk has been calculated and compared with similar scenarios in the absence of snow covered surfaces.

7.1 Previous Works

Vapor cloud explosions are a major hazard in most of oil and gas facilities [63, 64]. The vapor cloud generated shockwave is the most important characteristic of an explosion which determines the level of damage. Thus, in explosion modeling, the goal is to provide generated overpressure and then convert it into measureable losses in term of damage or fatality. For explosion modeling, empirical models are widely used [65]. However, most of these models and

tools are not suitable for explosion modeling in Arctic regions due to snow and ice covered surfaces. In addition to snow and ice covered surfaces, high levels of humidity and the presence of snow and ice particles in the air are the main characteristics of arctic regions [1]. While the effects of water vapor and droplets on the explosion have been well studied [66-68]; the impact of snow covered surfaces on the explosion behavior is less known and not been studied specially in the case of risk assessment. The behavior of snow and its coupling with overpressure blasts have been mostly studied in avalanche related researches [69] and is a newly opened area for risk assessment studies. Brown has shown that Jump equations can precisely describe the behavior of snow surfaces subjected to overpressure and shockwave [70, 71]. Later, Johnson et al. experiments confirmed Brown's methodology and showed that shockwave attenuates rapidly in snow due to momentum dissipation in snow and the compaction of snow [72]. The compaction of snow and snow surface displacement highly depends on the snow density and its initial properties [70, 71].

Despite the availability of the models described in chapter 5, there are certain scenarios and situations which require the model to be modified. An example of such situation is explosion hazards in a process industry or platform in arctic region. If the ground is covered with snow layer, explosion phenomena and subsequently generated overpressure differ compared to uncovered surfaces. For these cases if a snow layer is new and has low density, a considerable portion of energy is dissipated in snow. Simultaneously the snow is compacted and deformed due to the generated overpressure and the shock wave losses a portion of its energy. Coupling of transport phenomena and solid deformation is required for the case of explosion in arctic regions. However, coupling also introduces new sources of uncertainty into modeling [73].

High ambient air density, the presence of water and ice particles in air, low temperature and snow/ice covered surfaces are unique to Arctic regions. This study focuses on the impact of snow covered surfaces. A new methodology is proposed which couples Baker-Strehlow model with jump equations to predict the response of snow to shockwave and to modify overpressure profile. The proposed method is a new and simple approach to model explosion in arctic conditions.

7.2 Modeling

7.2.1 Baker-Strehlow Model

In the Baker-Strehlow model, the first step is to determine the fuel activity, obstruction density and flame expansion. Fuel activity depends on the flammable vapor, as fuel activity increases, the intensity of explosion increases. In the Baker-Strehlow model there are three levels of fuel reactivity: low, medium and high. For example, methane has a low fuel activity while hydrogen has a high fuel activity. Obstruction density depends on the congestion and confinement of scenario and has a direct effect on the intensity of explosion. Like fuel activity, there are three different levels of obstruction density: low, medium and high. The confinement and congestion also determines flame expansion modes on the spatial directions in which flame can expand. There are three modes of flame expansion: 1D, 2D and 3D. For example if explosion occurs in a long tunnel, flame expansion is 1D, propagating along the length of the tunnel. In contrast, a completely unconfined vapor cloud explosion flame expansion is 3D. Flame expansion is reversely proportional to the intensity of explosion: as flame has more ways for expansion, the generated overpressure is less. Explosion efficiency and ambient pressure are the other parameters which impact the consequence. For most practices, an efficiency of 30% is considered sufficient for conservative calculations. The explosion efficiency factor is included

for the fact that not all flammable gas contribute to explosion; not all the released energy is transformed to shockwave.

The next step is to determine the size of vapor cloud and released energy. The size of vapor cloud depends on the confined and congested areas, while the released energy is determined based on the combustion energy of fuel. Environment; climatic conditions will also impact conditions the released energy. For example for a partially confined area in a high wind, the concentration and subsequently mass fraction of fuel in the cloud will be very different than a low wind situation.

Baker-Strehlow model estimates scaled overpressure as a function of scaled distance for different flame speeds. Flame speed is determined based on the flame expansion, fuel reactivity and congestion. For each parameter, there are three different categories; thus, totally there are 27 different flame speeds. Eqs (54 and 55) show the distance and overpressure scaled relations respectively:

$$P_s = \frac{P_o}{P_a} \tag{54}$$

$$X_s = x(\frac{E}{P_a})^{\frac{-1}{3}} \tag{55}$$

Where P_s, P_o, P_a, X_s, x and E stand for scaled overpressure, generated overpressure, ambient pressure, scaled distance, distance and released energy respectively. After determining the flame speed, and released energy, the generated overpressure is estimated by graphs or corresponding correlations.

Eq. (56) shows these correlations and related coefficients are listed in Table 7.1.

$$P_s = \begin{Bmatrix} D \quad if\ X_s < X_0 \\ AB^{(1/X_s)}C^{X_s} \quad if\ X_s \geq X_0 \end{Bmatrix} \tag{56}$$

Table 7.1: Constants for Eq. (56).

Constants\Flame Speed (Mach)	0.2	0.35	0.7	5.2
A	0.0335	0.1041	0.3764	0.2932
B	0.8359	0.8642	0.7439	1.339
C	-1.1192	-1.0568	-1.2728	-1.1591
D	0.065	0.22	0.65	20
X_0	0.35	0.32	0.3	0.16

Figure 7.1 outlines the overpressure calculation using Baker-Strehlow model illustrating its quick and direct approach. However, this model is unable to account the impacts of environmental conditions e.g. a snow layer; therefore, modifications are required in this model. In this study, the released energy decreases as the shockwave or overpressure pulse propagates in environment due to energy dissipation by snow. Therefore the actual energy which contributes into generation of overpressure decreases with distance. This dissipated energy is in the form of thermal and mechanical energy; however, since the explosion is a rapid phenomenon, thermal energy is considered negligible compared to mechanical energy. Therefore the dissipated energy in this model is mechanical energy due to movement and deformation of snow. Eq. (57) presents the modified relation for released energy.

$$E(x) = E_0 - d(x) \tag{57}$$

Where E(x), E_0 and d(x) are corrected released energy for distance(x), initially released energy and dissipated energy until distance x from the center of explosion respectively.

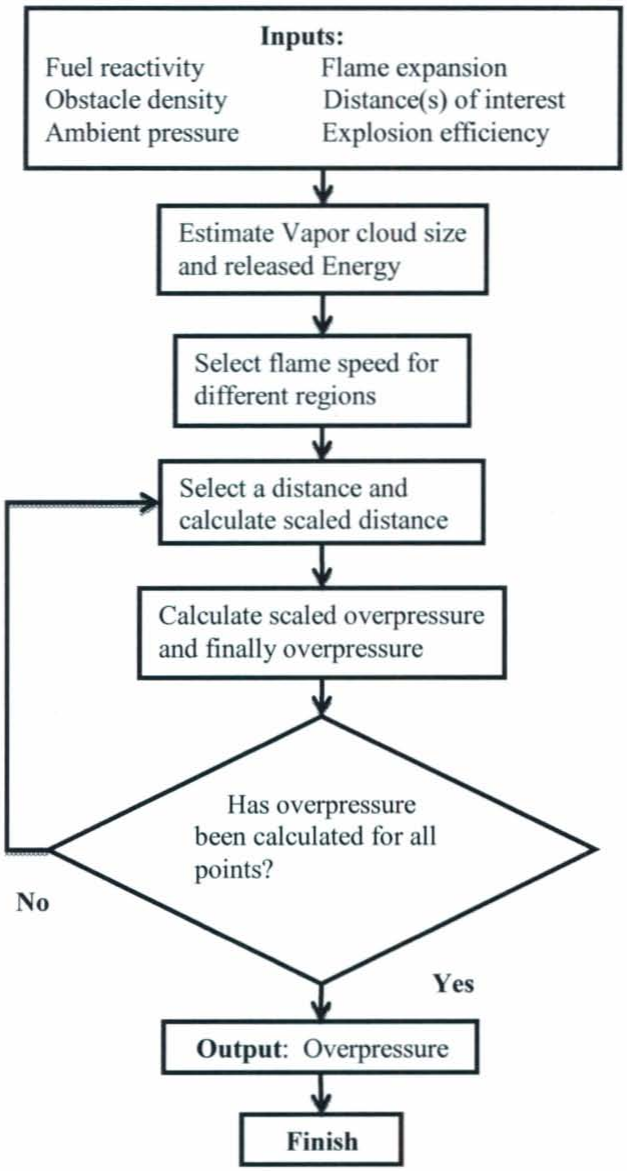

Figure 7.1: Flow chart for overpressure calculation by Baker-Strehlow model.

7.2.2 The New Model

The dissipated energy is calculated through the application of Jump equations (Eqs. (58-65)). Jump equations represent snow as a rate sensitive and nonlinear material. For overpressure which causes the inelastic behavior, snow response could be written as:

$$P_o = \frac{2\gamma J exp\,(-\emptyset^{\frac{\alpha}{\alpha_0}})}{3\alpha}\ln(\frac{\alpha}{\alpha-1}) + \frac{\tau}{\alpha}\left(- \frac{\partial^2\alpha}{\partial t^2} f(\alpha) + \frac{\left(\frac{\partial\alpha}{\partial t}\right)^2}{6} g(\alpha) \right) \quad (58)$$

where

$$\tau = \rho_m \frac{{\alpha_0}^2}{3(\alpha-1)^{\frac{2}{3}}} \quad (59)$$

$$f(\alpha) = (\alpha-1)^{\frac{-1}{3}} - (\alpha)^{\frac{-1}{3}} \quad (60)$$

$$g(\alpha) = (\alpha-1)^{\frac{-4}{3}} - (\alpha)^{\frac{-4}{3}} \quad (61)$$

In these equations γ, J and $\emptyset$ are snow constants and a_0 is the initial mean void radius considered 0.1 mm in this study. ρ_m is the ice density and the density ratio (α) is defined as:

$$\alpha = \frac{\rho_m}{\rho} \quad (62)$$

$\gamma = 3 * 10^7$ pa, J = 3.07, $\emptyset$ = 5.85, ρ_m= 1000 kg/m^3

Here α_0 is the initial density ratio of snow and ρ is the snow density.

Brown has shown that Eqs. (58-61) accurately model snow responses to a variety of pressure shockwaves and densities. The mass and momentum equation can be written as:

$$\frac{-\partial P_o}{\partial X} = \rho_0 \frac{\partial v}{\partial t} \tag{63}$$

and

$$\frac{\partial v}{\partial X} = \frac{1}{\alpha_0} \frac{\partial \alpha}{\partial t} \tag{64}$$

Differentiation of Eq. (64) with respect to time and substituting in Eq. (63) results in:

$$\frac{-1}{\rho_0} \frac{\partial^2 P_o}{\partial X^2} = \frac{1}{\alpha_0} \frac{\partial^2 \alpha}{\partial t^2} \tag{65}$$

This equation is the familiar form of a wave equation and was used along with Eqs. (58-62) to investigate the response of snow to applied external overpressures. It could be done by substitution of Eq. (58) into Eq. (65) to have a forth order non-linear partial differential equation for α. X is the direction of wave propagation and the direction of snow depth.

$$\frac{-1}{\rho_0} \frac{\partial^2 \left\{ \frac{2\gamma J exp\left(-\emptyset^{\frac{\alpha}{\alpha_0}}\right)}{3\alpha} \ln\left(\frac{\alpha}{\alpha - 1}\right) + \frac{\tau}{\alpha} \left(- \frac{\partial^2 \alpha}{\partial t^2} f(\alpha) + \frac{\left(\frac{\partial \alpha}{\partial t}\right)^2}{6} g(\alpha) \right) \right\}}{\partial X^2} = \frac{1}{\alpha_0} \frac{\partial^2 \alpha}{\partial t^2} \tag{66}$$

Figure 7.2 illustrates the algorithm of the proposed method. In each step, jump equations are used to calculate the dissipated energy. Based on dissipated energy, released energy is modified and subsequently used in the Baker-Strehlow model to calculate corrected overpressure. Each

step of these calculations is computationally expensive especially in comparison to the simple Baker-Strehlow method.

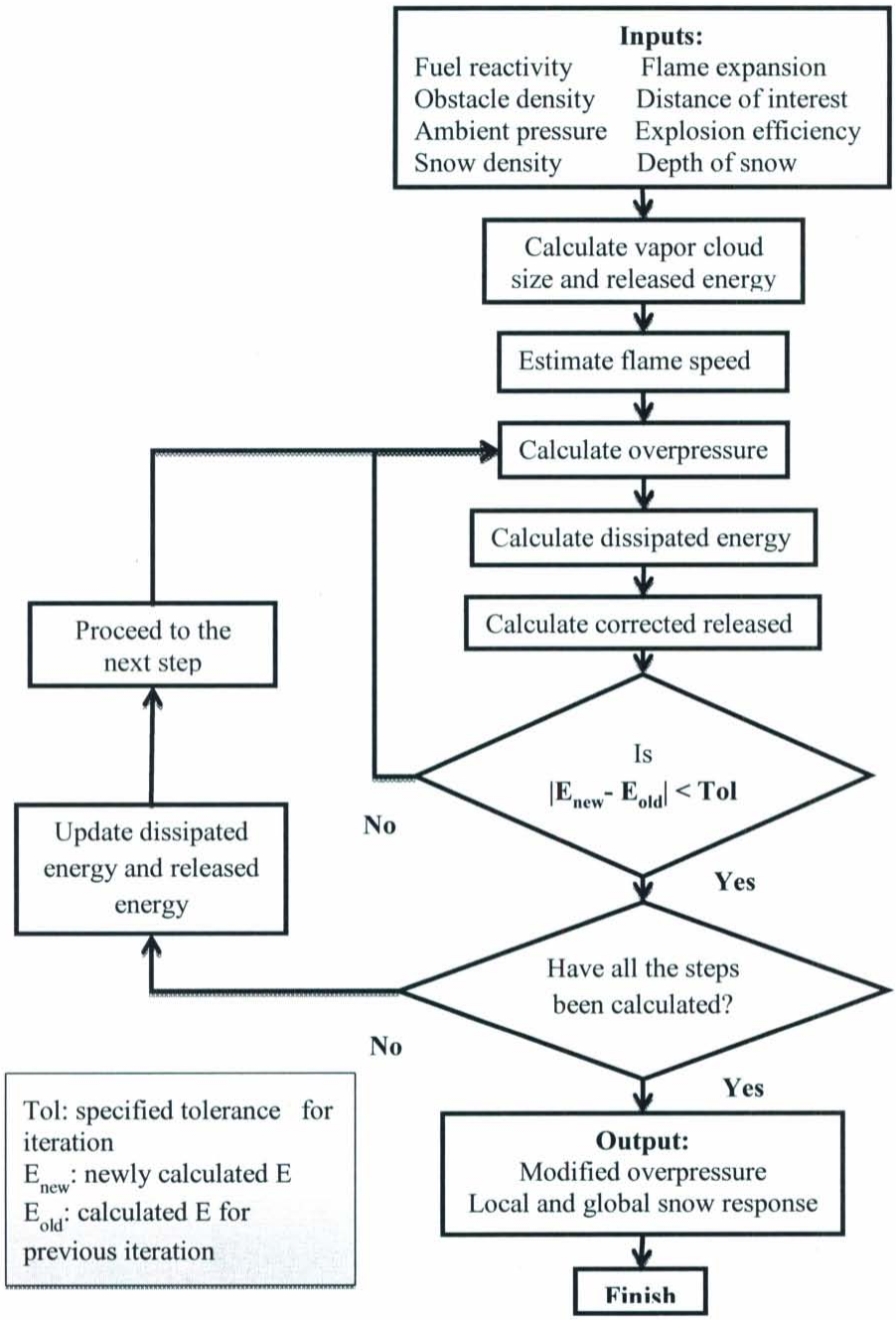

Figure 7.2: Flowchart for overpressure calculation using the new model.

To quantitavely compare the results of new approach, the risk is calculated which is defined as:

$$R(D_d) = \int_0^{D_d} P_o \, dx \tag{67}$$

Where D_d is the desired distance,P_o is the peak overpressure for any distance x and $R(D_d)$ is the cumulative overpressure which causes damages up to desired distance.

7.3 Results and Discussions

The solution of Jump equations provides unique information regarding the snow behavior. These equations are able to correctly represent both local and global behaviors of snow with respect to its depth and density e.g. density changes, compaction, deformation and energy dissipation. The local behavior captures how snow density changes in the direction of its depth while global behavior indicates how snow surface is displaced with respect to the direction(s) of overpressure propagation and its effects on energy dissipation.

Figures 7.3 and 7.4 present the variation of snow density in depth axis for initial density equal to 125 and 250 kg/m^3 respectively. A quick comparison between these cases reveals that as the density increases, the rate of compaction decreases. Figure 7.5 shows such a comparison. This figure compares the variation of density when the initial density has been reduced by from 250 kg/m^3 to 125 kg/m^3. For this figure, applied overpressure is the same as applied overpressure for Figures 7.3 and 7.4. The bulk of deformation and displacement is higher early. Furthermore, it is expected that up to a certain value as snow density decreases, more energy is dissipated. Moreover for any case, after a while density growth and snow displacement becomes negligible. For instance, after 0.5 second there is no significant snow compaction at depth of 0.95 m.

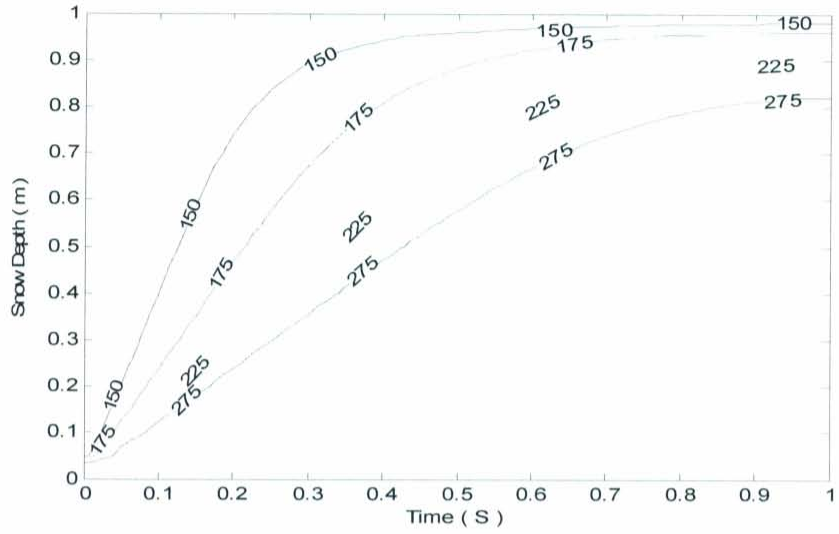

Figure 7.3: Snow compaction in depth, initial snow density = 125 kg/m^3 and applied overpressure = 10 bar.

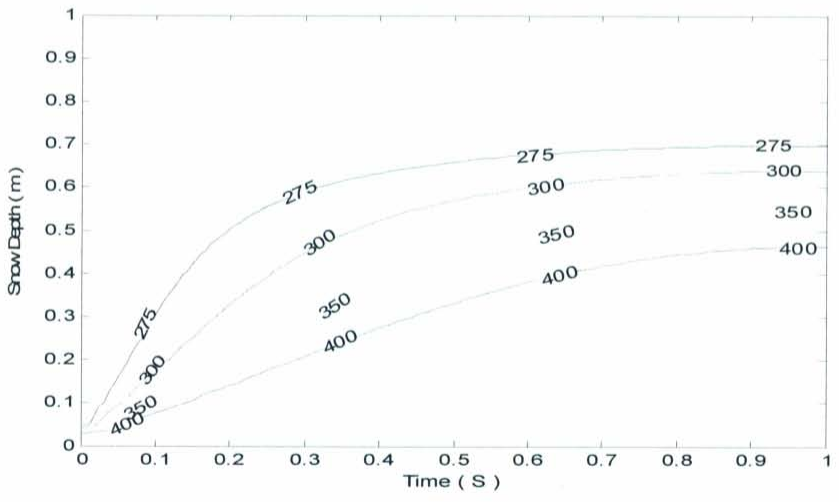

Figure 7.4: Snow compaction in depth, initial snow density = 250 kg/m^3 and applied overpressure = 10 bar.

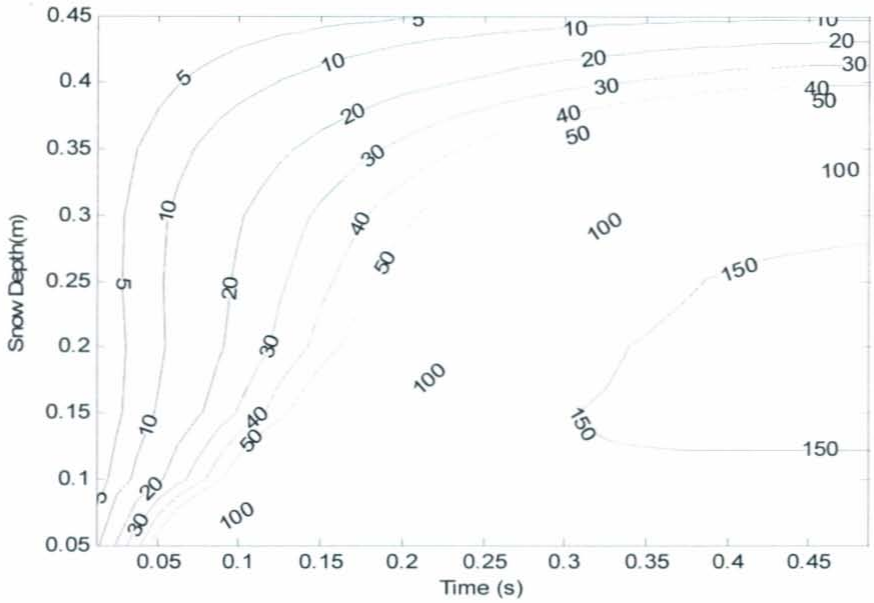

Figure 7.5: Comparison of the rate of density change (Initial snow density = 125 kg/m^3 – Initial snow density = 250 kg/m^3).

It is logical to expect that as applied load (overpressure) decreases, the rate of compaction changes and displacement decreases; therefore, the dissipated energy decreases as well. Figure 7.6 illustrates snow behavior for a lower applied overpressure. In comparison to Figure 7.3, just applied overpressure has decreased. This figure confirms that as overpressure decreases, rate of density changes reduces dramatically.

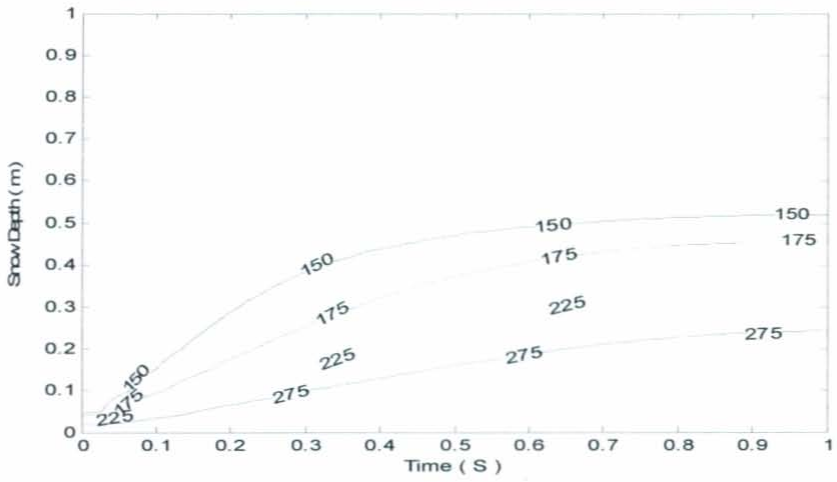

Figure 7.6: Snow compaction in depth when the applied overpressure is equal to 1 bar; initial snow density = 125 kg/m^3.

The effect of depth on the local behavior of snow has been shown in Figures 7.7 and 7.8. For these figures, all parameters are similar to the parameters in Figure 7.3 except the depth of snow. As depth of snow decreases, with the same conditions, the shockwave faster reaches to the hard and incompatible hard surface which is below snow layer. This results into a higher rate of compaction and also a shorter stability time. For instance, the density of last 5 cm of snow does not change after 0.4 second when depth is equal to 25 cm.

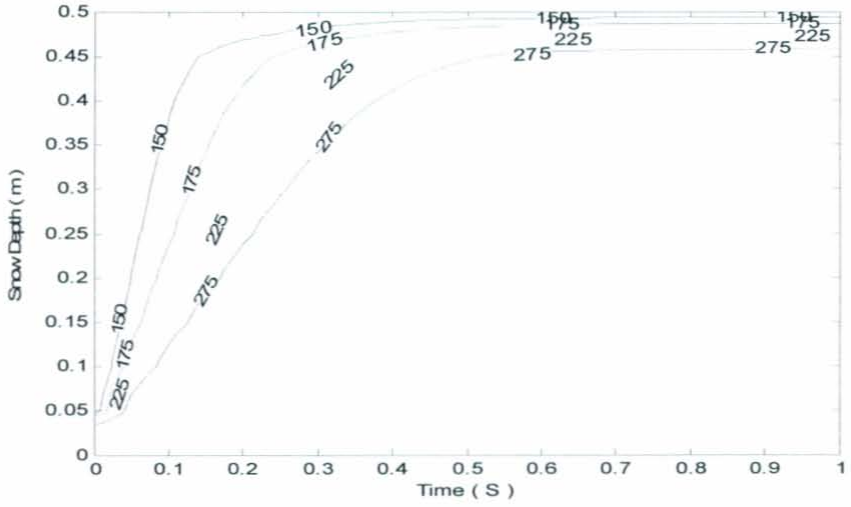

Figure 7.7: Local behavior of snow when snow depth = 0.5 m.

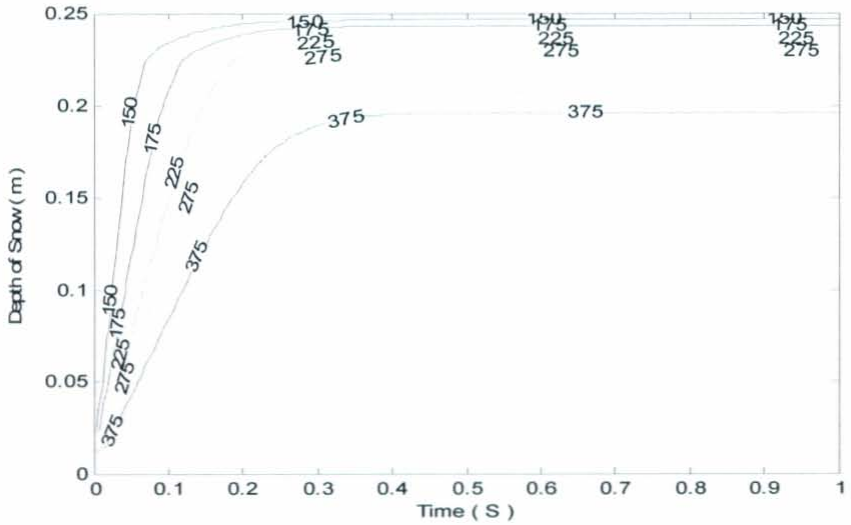

Figure 7.8: Local behavior of snow when depth = 0.25 m.

The application of proposed method is shown through a case study and the results are shown in Fig 7.9-7.13. In this case the assumption is that there is no wind. Moreover, there is a

homogenous layer of snow with the depth of 0.5 m. Furthermore, this case assumes that there is enough fuel concentration and congestion to create a high overpressure in the center of explosion.

As the shockwave propagates, it loses a portion of its energy due to snow deformation. Therefore, the overpressure for far fields is expected to be less than what a simple model like Baker-Strehlow predicts. In the center and near fields, energy dissipation is larger because of generation of larger overpressure. Figure 7.9 shows snow displacement and its final depth for several different initial densities. As density decreases, the displacement of the snow surface is larger and subsequently, energy dissipation is larger.

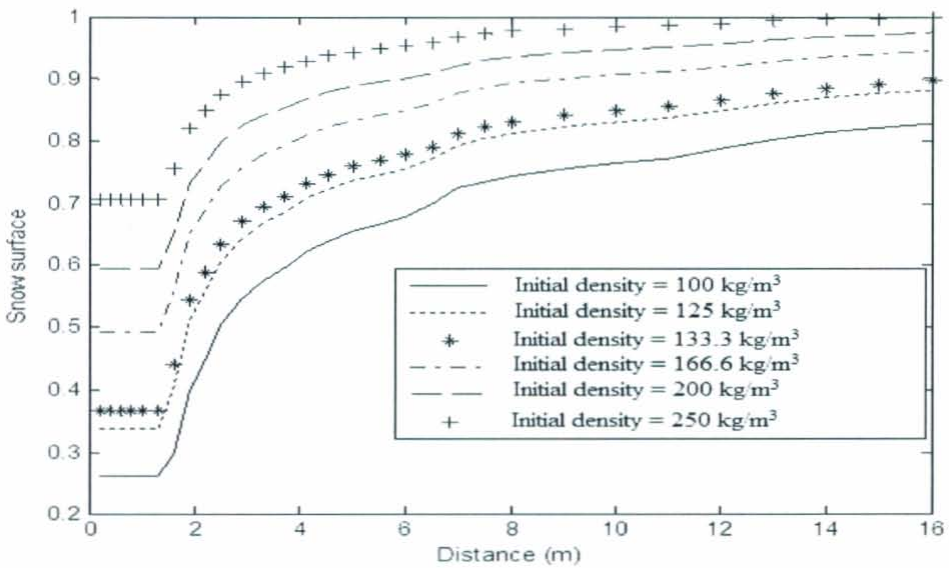

Figure 7.9: Snow surface displacement due to shockwave interaction.

Although, snow may deformed severely in distances close to the explosion center, the dissipated energy is relatively small in comparison to the initial explosion released energy. This

is mainly because in near field the surface of displaced snow is low and in the far field snow is not affected significantly. However, the snow layer results in lower generated overpressure. Figures 7.10- 7.12compare generated overpressure for different cases in closed distances (< 4.0 m), medium distances (< 25.0 m) and far field (< 250.0 m) respectively.

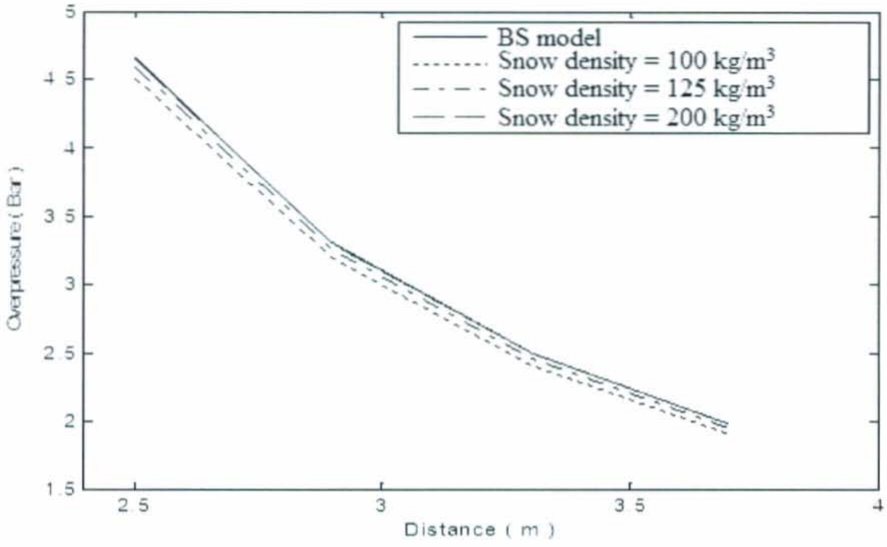

Figure 7.10: Comparison between overpressure of several cases for close distances

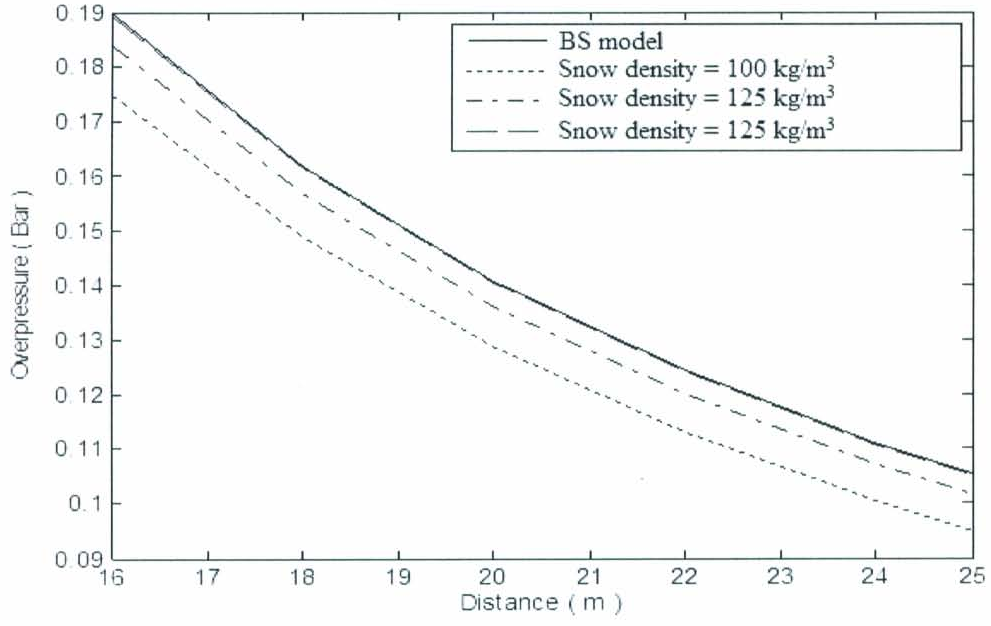

Figure 7.11: Pick overpressure over snow for several different snow densities in comparison to Baker-Strehlow model for medium distances.

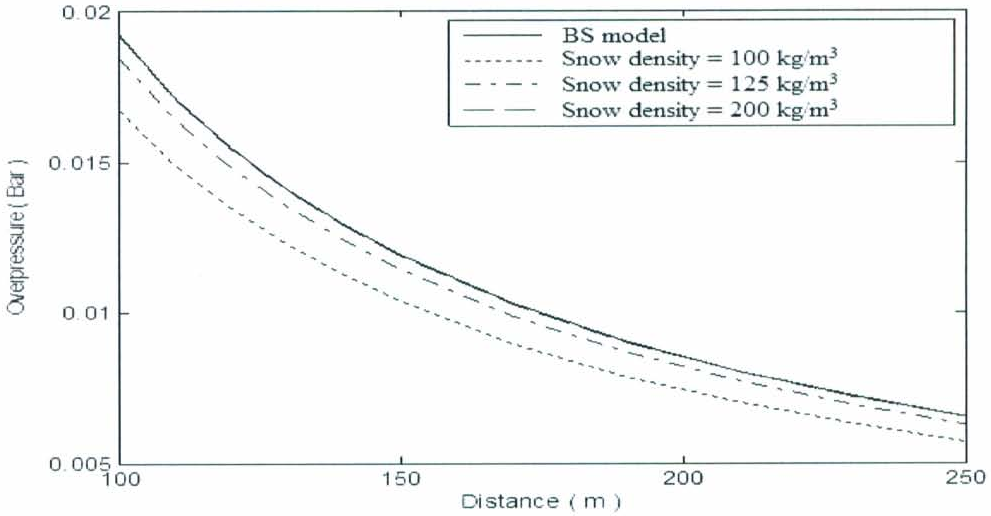

Figure 7.12: Comparison between overpressure of several cases in far distances.

A comparison between result of Baker-Strehlow method and this new method reveals that there is a considerable difference in the calculated overpressure. Figures 7.10-7.12 show that generated overpressure over snow covered surfaces is less than no snow covered surfaces at any distance. Moreover, these figures illustrate that as snow density increases, differences between the Baker-Strehlow model and the proposed method decreases. In other word, as the density of snow increases, the results of proposed method become closer to the results of the Baker-Strehlow method. The reason of such behaviors is that as snow density increases, compaction and subsequently dissipated energy becomes less significant compared to initial released energy. Figure 7.13 presents risk comparison for different cases based on the definition which is given in methodology section. Results show reduction in risk, although the differences may not be significant. Moreover, this figure illustrates that presence of snow layer does no significant effects on the overpressure and risk level of near fields. It is mainly because the dissipated energy is relatively small in comparison to released energy.

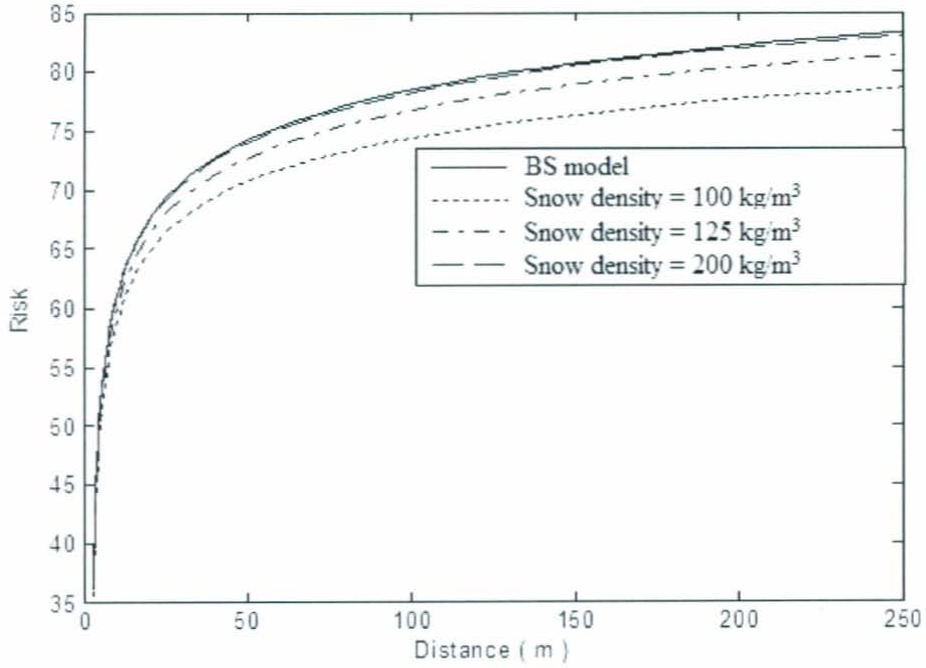

Figure 7.13: Risk level versus distance for different cases.

Chapter 8: Conclusions

This chapter consists of two parts. In the first part, the summary and conclusion of the thesis is presented. The next part includes suggestions and recommendations for future works.

8.1 Summary and Conclusion

This thesis was focused on the Arctic region. Due to unique environmental characteristics of the Arctic region, the usually practiced models cannot be used for this region. Therefore, in this study two models were revised and developed to account for the environmental uniqueness.

A new methodology was proposed to model pool fires in the arctic region. The Fay model is revised and extended to account for surface reflectivity and the presence of water/ice particles in the air. As a result, the revised model is effective in a region like arctic where surface reflectivity and the presence of droplets are the main environmental parameters. Furthermore, the revised model is extended to account for the radiation from the plume zone. Although, the thermal radiation from this zone is small compared to the combustion zone; plume zone still has an important role especially for large heights. The results of the revised model show that thermal radiation profile in arctic region is significantly different compared to moderate regions. This difference could significantly affect the consequence and subsequently the final outcomes and decisions of risk assessment.

A new model is presented for calculating explosion overpressure in the arctic region. In this new model, the Baker-Strehlow model has been coupled with jump equations to calculate energy dissipating due to snow compaction. Finite difference schemes are used to solve the partial differential equations resulting from this coupling. The results show that overpressure in the

arctic region is lower compared to temperate climates. The reason is snow compaction and energy dissipation due to snow deformation. Furthermore, as the snow layer density increases, energy dissipation becomes negligible. This means that the difference in the generated overpressures between arctic region and temperate regions decreases.

8.2 Suggestions for Future Works

The pool fire model proposed in this thesis is applicable to steady state situation when the fire is fully developed but not appropriate for the initial growths or final quenching. Although the steady state step is the most hazardous phase during the burning of a fuel, it is worthwhile to further extend this model to include fire growth and quenching.

Thermal radiation has not been included in the energy conservation equations for the proposed pool fire model. Including thermal radiation in the energy conservation calculations would require an iterative method to reach a solution. Although this results into a longer simulation time, it would improve the accuracy of calculations.

Unlike the pool fire model, the proposed explosion model only accounts for snow compaction and ignores environmental variables like temperature and the presence of droplet in the air. This limitation goes back to the Baker-Strehlow model as it does not account for environment temperature or the presence of droplets in the air. Therefore the proposed model for the explosion could be further expanded by including the effect of other environmental parameters on the explosion intensity.

Models for other accidental fires like jet fire and BLEVE should be developed based on the unique characteristics of the Arctic region.

Bibliography

[1] M.C. Serreze and R.G. Barry. The Arctic Climate System. Cambridge: Cambridge university press, 2005.

[2] D. Cimini, E. Westwater and A.J. Gasiewski. "Recent Progress in temperature and humidity profiling in the Arctic using millimeter-wave radiometry", Proceedings of the 8th International Symposium on Tropospheric Profiling, Delft, The Netherlands, October 2009.

[3] M.S. Timlin and J.E. Walsh. "Historical and Projected Distributions of Daily Temperature and Pressure in the Arctic", *Arctic*, vol. 60, pp. 389-400, 2007.

[4] J.E. Overland. "Meteorology of the Beaufort Sea". Journal of Geophysical Research, vol. 114, pp. 1-10, 2009.

[5] R. Treffeisen, R. Krejci, J. Strom, A.C. Engvall, A. Herber and L. Thomason. "Humidity observations in the Arctic troposphere over Ny-Alesund, Svalbard based on 15 years of radiosonde data". Atmospheric Chemistry and Physics, vol. 7, pp. 2721-2732, 2007.

[6] N.S. Arunarj and J. Maiti. "A methodology for overall consequence modeling in chemical industry". Journal of Hazardous Materials, vol. 169, pp. 556-574, 2009.

[7] R. Pula, F. Khan, B. Veitch and P. Amyotte. "Revised fire consequence models for offshore quantitative risk assessment". Journal of Loss Prevention in the Process Industries, vol. 18, pp. 443-453, 2005.

[8] R. Pula, F. Khan, B. Veitch and P. Amyotte. "A grid based approach for fire and explosion consequence analysis". Process Safety and Environmental Protection, vol. 84(B2), pp. 79-91, 2006.

[9] M. Hightower et al. Guidance on risk analysis and safety implications of a Large Liquefied Natural Gas (LNG) spill over water. Oak Ridge: SANDIA Lab, 2004.

[10] M.G. Mares, L. Zarate and J. Casal. "Jet Fire and the Domino Effect". Fire Safety Journal, vol. 43, pp. 583-588, 2008.

[11] G. Hankinson, B.J. Lowesmith, J.A. Evans and L.C. Shirvill. "Jet Fire Involving Releases of Crude Oil, Gas and Water". Process Safety and Environmental Protection, vol. 85(B3), pp. 221-229, 2007.

[12] M.G. Mares, M. Munoz, and J. Casal. "Radiant Heat from Propane Jet Fire". Experimental Thermal and Fluid Science. vol. 34, pp. 323-329, 2010.

[13] A.M. Brik, C. Davison and M. Cunningham. "Blast Overpressure from Medium Scale BLEVE Tests". Journal of Loss Prevention in Process Industries, vol. 20, pp. 194-206, 2007.

[14] G.M. Makhviladze and S.E. Yakush. "Blast Waves and Fireballs from Bursts of Vessels with Pressure-Liquefied Hydrocarbons". Proceedings of the Combustion Institute, vol. 29, pp. 313-320, 2002.

[15] Z. Fu, and G. Hadjisophocleous. "A Two-Zone Fire Growth and Smoke Movement Model for Multi-Compartment Buildings". Fire Safety Journal, vol. 34, pp. 257-285, 2000.

[16] W.D. Walton. "Zone Computer Fire Models for Enclosures" in SFPE Handbook of Fire Protection Engineering, 2nd Edition, P.J.D. Nenno, Chapter 7, Section 3, pp. 3/148-151, 2002.

[17] C. Xiaojun, Y. Lizhong, D. Zhihua and F. Weicheng. "A Multi-Layer Zone Model for Predicting Fire Behavior in a Fire Room". Fire Safety Journal, vol. 40, pp. 267-281, 2005.

[18] N.P. Komninos. "Modeling HCCI Combustion: Modification of a Multi-Zone Model and Comparison to Experimental Results at Varying Boost Pressure". Applied Energy, vol. 86, pp. 2141-2151, 2009.

[19] R. Friedman. "An International Survey of Computer Models for Fire and Smoke". Journal of Fire Protection Engineering, vol. 4, pp. 81-92, 1992.

[20] S. M. Olenick, D. J. Carpenter. "An Updated International Survey of Computer Models for Fire and Smoke". Journal of Fire Protection Engineering, vol. 13, pp. 87-110, 2003.

[21] C.E. Lynch and M.J. Smith. "Hybrid RANS-LES Turbulence Models on Unstructured Grids", 38th Fluid Dynamics Conference and Exhibit, Seattle, Washington, 2008.

[22] P. Moin and K. Mahesh. "Direct Numerical Simulation: a Tool in Turbulence Research". Annuals Review of Fluid Mechanics, vol. 30, pp. 539-578, 1998.

[23] T. Kobsyashi "Large Eddy Simulation for Engineering Applications". Fluid Dynamics Research", vol. 38, pp. 84-107, 2008.

[24] J. Meyers, B.J. Geurts and M. Baelmans. "Database Analysis of Errors in Large Eddy Simulation". Physics of Fluids, vol. 15, pp. 2740-2755, 2003.

[25] W.K. Chow "A Comparison of the Use of Fire Zone and Field Models for Simulating Atrium Smoke-Filling Processes". Fire Safety Journal, vol. 25, pp. 337-353, 1995.

[26] K.S. Mudan. "Thermal Radiation Hazards from Hydrocarbon Pool Fires". Progress in Energy and Combustion Science, vol 10. pp. 59-80, 1984.

[27] P. Joulain. "The Behavior of Pool Fires: State of The Art and New Insights". 27th symposium on combustion, The Combustion Institute, Pages 2691-2706, 1998.

[28] P.J. Rew, W.G. Hulbert and D.M. Deaves. "Modeling of Thermal Radiation from External Hydrocarbon Pool Fires". Trans IChemE, vol. 75 (B), pp. 81-89, 1997.

[29] P. Joulain. "Convective and Radiative Transport in Pool and Wall Fires: 20 Years of Research in Poitiers". Fire Safety Journal, vol. 26, pp. 99-149, 1996.

[30] B.J. McCaffrey. "Momentum Implications for Buoyant Diffusion Flames", Journal of Combustion and Flame, vol. 52, pp. 149-167, 1983.

[31] S.J. Fischer, B.H. Duparc and W.L. Grosshandler. "The Structure and Radiation of an Ethanol Pool Fire". Journal of Combustion and Flame, vol. 70, pp. 291-306, 1987.

[32] P.K. Raj. "Large Hydrocarbon Fuel Pool Fires: Physical Characteristics and Thermal Emission Variation with Height". Journal of Hazardous Materials, vol. 140, pp. 280-292, 2007.

[33] J.A. Fay. "Model of Large Pool Fires". Journal of Hazardous Materials, vol. 136 (B), pp. 219-232, 2006.

[34] H. Chun, K. Wehrstedt, I. Vela and A. Schonbucher. "Thermal Radiation of di-tert-butyl Peroxide Pool Fires: Experimental Investigation and CFD Simulation". Journal of Hazardous Materials, vol. 167, pp. 105-113, 2009.

[35] K.A. Jensen, J.F. Ripoll, A.A. Wary, D. Joseph and M.E. Hafi. "On Various Modeling Approaches to Radiative Heat Transfer in Pool Fires". Combustion and Flame, vol. 148, pp. 263-279, 2007.

[36] A.T. Modak. "Thermal Radiation from Pool Fires", Combustion and Flame, vol. 29, pp. 177-192, 1977.

[37] L. Orloff. "Simplified Radiation Modeling of Pool Fires". 18th Symposium on Combustion, the Combustion Institute, pp. 549-561, 1981.

[38] A. Hamins, M. Klassen, J. Gore and T. Kashiwagi. "Estimate of Flame Radiation via a Single Location Measurement in Liquid Pool Fires". Combustion and Flame, vol. 86, pp. 223-228, 1991.

[39] G. Krishnamoorthy. "A Comparison of Gray and Non-Gray Modeling Approaches to Radiative transfer in Pool Fire Simulations". Journal of Hazardous Materials, vol. 182, pp. 570-580, 2010.

[40] M.B. Kim, Y.J. Jang and J.K. Kim. "Burning Rate of a Pool Fire with Downward-Directed Sprays". Fire Safety Journal, vol. 27, pp. 37-48, 1996.

[41] J.C. Chang, C.M. Lin and S.L. Huang. "Experimental Study on the Extinction of Liquid Pool Fire by Water Droplet Streams and Sprays". Fire Safety Journal, vol. 42, pp. 295-309, 2007.

[42] B. Chen, S.X. Lu, C.H. Li, Q.S. Kang and V. Lecoustre. "Initial Fuel Temperature Effects on Burning Rate of Pool Fire". Journal of Hazardous Materials, vol. 188, pp. 369-373, 2011.

[43] T.S. Ravigururajan and M.R. Beltran. "A Model for Attenuation of Fire Radiation through Water Droplets". Fire Safety Journal, vol. 15, pp. 171-181, 1989.

[44] G.N. Mercer and R.O. Weber. "Plumes above Line Fires in a Cross Wind". int. J. wildland fire, vol. 4, pp. 201-207, 1994.

[45] E. Gramsch, L. Catalan, I. Ormeno and G. Palma. "Traffic and Seasonal Dependence of the Light Absorption Coefficient in Santiago De Chile". Applied Optics, vol. 39, pp. 4895-4901, 2000.

[46] C. Doolan. "The Effect of Water Mist and Water Spray on Radiative Heat Transfer for Stored Ordnance". Defense Science and Technology Organization, 2003.

[47] W.M. Irvine. "Infrared Optical Properties of Water and Ice Spheres". ICARUS, vol. 8, pp. 324-360, 1968.

[48] S. Hostikka and K. McGrattan. "Numerical Modeling of Radiative Heat Transfer in Water Sprays". Fire Safety Journal, vol. 41, pp. 76-86, 2006.

[49] V.M. Zolotarev, B.A. Mikhilov, L.L. Alperovich and S.I. Popov, Dispersion and absorption of liquid water in the infrared and radio regions of the spectrum, Optics and Spectroscopy, vol. 27, pp. 430-432, 1969.

[50] G.M. Hale and M.R. Querry. "Optical constants of water in the 200 nm to 200 μm wavelength region". Applied Optic, vol. 12, pp. 555-563, 1973.

[51] P. Schiebener, J. Straub, J.M. Sengers and J.S. Gallagher. "Refractive index of water and steam as function of wavelength, temperature and density". Journal of Physical and Chemical Reference Data, vol. 19, pp. 677-717, 1990.

[52] C.J. Lea. "A Review of the State-of-the-Art in Gas Explosion Modeling", HSL Report, 2002.

[53] A.C. Berg van den and A. Lannoy. "Methods for Vapor Cloud Explosion Blast Modeling". Journal of Hazardous Materials, vol. 34, pp. 151-171, 1993.

[54] B.J. Wiekema. "Vapor Could Explosion Model". Journal of Hazardous Materials, vol. 3, pp. 221-232, 1980.

[55] A.C. Berg van den. "The Multi Energy Method. A Framework for Vapor Cloud Explosion Blast Prediction". Journal of Hazardous Materials, vol. 12, pp. 1-10, 1985.

[56] Q.A. Baker, M.J. Tang, E.A. Scheier and G.J. Silvia. "Vapor Cloud Explosion Analysis". Journal of Process Safety Progress, vol. 15, pp. 106-109, 1996.

[57] Q.A. Baker, C.M. Doolittle, G.A. Fitzgerald and M.J. Tang. "Recent Developments in the Baker-Strehlow VCE Analysis Methodology". Journal of Process Safety Progress, vol. 17, pp. 297-301, 1998.

[58] M.J. Tang and Q.A. Baker. "A New Set of Blast Curves from Vapor Cloud Explosions". Journal of Process Safety Progress, vol. 18, pp. 235-240, 1999.

[59] M.J. Tang and Q.A. Baker. "Comparison of Blast Curves from Vapor Cloud Explosions". Journal of Loss Prevention in Process Industries, vol. 13, pp. 433-438, 2000.

[60] S.H. Ledin. Review of COMEX and NVBANG Explosion Models. HSL Report, 2004.

[61] R.S. Cant, W.N. Dawes and A.M. Savill. "Advanced CFD Modeling of Accidental Explosions". Annual Review of Fluid Mechanics, vol. 36, pp. 97-119, 2004.

[62] N.R. Popat. "Investigation to Improve and assess the Accuracy of Computational Fluid Dynamics Based Explosion Model". Journal of Hazardous Materials, vol. 45, pp. 1-25, 1996.

[63] D. Bjerketvedt, J.R. Bakke and K.V. Wingerden. "Gas Explosion Handbook". Journal of Hazardous Materials, vol. 52; pp. 1-150, 1997.

[64] C.C. James and J.A. Krembs, Large Property Damage Losses in the Hydrocarbon-Chemical Industries—A Thirty-Year Review. Marsh Consulting Risk, Nineteenth Edition, 2001.

[65] H.S. Ledin and C.J. Lea. "A Review of the State-of-the-Art in Gas Explosion Modeling". HSL Report, 2002.

[66] D. Schwer and K. Kailasantah. "Blast Mitigation by Water Mist: Simulation of Confined Blast Waves". Naval Research Laboratory Report, MR/6410-03-8658, 2001.

[67] D. Schwer and K. Kailasantah. "Blast Mitigation by Water Mist: Mitigation of Confined and Unconfined Blasts". Naval Research Laboratory Report, MR/6410-06-8976, 2006.

[68] K.C. Adiga, H.D. Willauer, R. Ananth and F.W. Williams. "Droplet Breakup Energies and Formation of Ultra-fine Mist". Suppression and Detection Research and Applications- A Technical working Conference (SUPDET 2007), 2007.

[69] E.R. Lachapelle. "Alternative Methods for the Artificial Release of Snow Avalanches". Journal of Glaciology, vol. 19, pp. 419-429, 1977.

[70] R.L. Brown. "An Analysis of Non-Steady Plastic Shock Wave in Snow". Journal of Glaciology, vol. 25, pp. 279-287, 1980.

[71] R.L. Brown. "A Method for Evaluating Shockwave Propagation in Snow", Cold Regions Science and Technology, vol. 5, pp. 151-156, 1981.

[72] J.B. Johnson, D.J. Solie and S.A. Barrett. "The Response of a Seasonal Snow Cover to Explosive Loading". Annals of Glaciology, vol. 19, pp. 49-54, 1994.

[73] W.L. Oberkampf, S.M. Deland, B.M. Rutherford, K.V. Diegert and K.F. Alvin. "Error and Uncertainty in Modeling and Simulation". Reliability Engineering and Safety Systems, vol. 75, pp. 333-357, 2002.

Appendix A

$$\sigma T^4 \Delta A = \int_0^A \frac{\vec{n}.\overrightarrow{di}}{di} q''|_{di} dA; \qquad (\vec{n}.\overrightarrow{di}) > 0 \tag{A-1}$$

As $q''|_{di}$ is constant, we need to calculate the right side integral. If we transform this integral to spherical coordination, this integral can be written as

$$\int_0^A \frac{\vec{n}.\overrightarrow{di}}{di} dA = \int_0^A \cos(\theta)\cos(\varphi)\, dA \tag{A-2}$$

Where, θ and φ are azimuthal and polar angels respectively. The (dA) in this integral is equal to

$$dA = di\sin(d\theta)\, di\sin(d\varphi) = di^2 \sin(d\theta)\sin(d\varphi) \tag{A-3}$$

On the other hand, we know that

$$\lim_{x\to 0} \sin(x) = x \tag{A-4}$$

Using (Eq. A-4) in (Eq. A-3) and substituting into (Eq. A-2) results in

$$\int_0^A \cos(\theta)\cos(\varphi)\, dA = di^2 \int_{-\frac{\pi}{2}}^{\frac{\pi}{2}} \int_{-\frac{\pi}{2}}^{\frac{\pi}{2}} \cos(\theta)\cos(\varphi)\, d\theta\, d\varphi = 4di^2 \tag{A-5}$$

Replacing (Eq. A-5) into (Eq. A-1) results into

$$q''|_{di} = \frac{\sigma T^4 \Delta A}{4di^2} \tag{A-6}$$

Appendix B

For a Gaussian distribution, Probability Density Function (PFD) can be shown as

$$f(x) = \frac{1}{\sqrt{2\pi\sigma^2}} \exp\left(-\frac{(x-\mu)^2}{2\pi\sigma^2}\right) \qquad (B-1)$$

Where μ presents the mean value and σ^2 determines the width of distribution. "σ^2 equal to 0" mathematically means that all the droplets have a same diameter (μ). Then we have

$$m_d = \rho_d V_d = N\frac{4\pi\rho_d}{3}\mu^3 \qquad (B-2)$$

Where, V_d is occupied volume by droplets and N is the number of droplets per unit volume. Finally

$$A_d = N\pi\mu^2 = \frac{3m_d}{4\rho_d\mu} \qquad (B-3)$$